The Astrophysical Journal, 979:186 (16pp), 2025 February 1 https://doi.org/10.3847/1538-4357/ada0b9

Study on the Shallow Decay Segment of Gamma-Ray Burst X-Ray Afterglow

Litao Zhao, Minjiang Chen, Fan Wu, Yang Liu, Xuqing Wang, and Yuxin Wang
School of Mathematics and Science, Hebei GEO University, Shijiazhuang, People's Republic of China; zhaolt@mail.bnu.edu.cn
Received 2024 August 8; revised 2024 December 7; accepted 2024 December 15; published 2025 January 27

Abstract

The X-ray afterglow of a certain fraction of gamma-ray bursts (GRBs) comprises a phase of shallow decay. However, the origin of the shallow decay segment is still a mystery. In this paper, we select 103 GRBs that exhibit a shallow decay segment, based on Swift/XRT data prior to 2023 June. We apply the fallback accretion energy external dissipation model to the shallow decay segment in our sample, and find the model can interpret the shallow decay segment within a reasonable range of parameter space. The fallback rate of the progenitor envelope materials onto the accretion disk can reach a peak of 10^{-7}–0.1 $M_\odot$ s^{-1} within a time frame of 10–10^5 s, which is consistent with the typical density profile and spin profile of the progenitor of a GRB. During the fallback process of progenitor envelope materials, progenitor stars of most GRBs have the highest fallback rate at a radius ~10^{10} cm, which is consistent with the typical radius of a Wolf–Rayet star. The production of shallow decay segments of most GRBs in our sample requires injecting Blandford–Znajek (BZ) energy equal to 10–100 times the kinetic energy of the initial GRB blast wave into the blast wave. However, the shallow decay segment of a few GRBs requires the injected energy to be comparable to the kinetic energy of the blast wave, which means that even if less energy is injected into a GRB blast wave, it is still possible to produce a shallow decay segment. In addition, the peak time of the fallback rate of the progenitor envelope materials is close to the time when BZ energy is injected into the blast wave, which means that the fallback accretion is more active in the initial phase. In summary, our research results provide further support to an external origin for the shallow decay segment in GRBs.

Unified Astronomy Thesaurus concepts: Gamma-ray bursts (629)

Materials only available in the online version of record: figure sets

1. Introduction

A gamma-ray burst (GRB) is currently the most intense gamma-ray photon burst phenomenon observed since the Big Bang, and consists of two emission phases: the prompt phase and the afterglow phase. The prompt phase is defined as the time period during which a sub-MeV band detector detects emission above the instrument's background emission level, which may be related to internal energy dissipation of the GRB jet, such as internal shocks or magnetic reconnection processes. In addition, the afterglow phase is usually defined as the time period following the sub-MeV prompt phase in observations, and includes multiple bands of emission, which may be related to the external shock formed by the GRB jet as it moves through the circumburst medium (see B. Zhang 2018 for a review).

The discovery of afterglow brought GRB research to a climax and has greatly improved researchers' understanding of GRBs. Especially since the launch of Neil Gehrels Swift Observatory, more details of afterglow emission have been revealed thanks to its rapid response and accurate positioning abilities (D. N. Burrows et al. 2005; G. Tagliaferri et al. 2005; J. A. Nousek et al. 2006; P. T. O'Brien et al. 2006; B. Zhang et al. 2006; P. A. Evans et al. 2009). After accumulating six months of Swift/XRT data, B. Zhang et al. (2006) proposed a canonical light curve of X-ray afterglow, which includes the steep decay segment, the shallow decay segment, the normal decay segment, the post jetlike break decay segment, and the X-ray flare. Through the study of long GRBs, it was found that the rest-frame time at the end of the shallow decay segment of X-rays, t'_b, is roughly inversely correlated with its corresponding X-ray luminosity L_X (Dainotti relation), with a slope ~−1 (M. G. Dainotti et al. 2008, 2010, 2011). The Dainotti relation has been interpreted in the context of the central engine of both a hyperaccreting black hole (BH; J. K. Cannizzo & N. Gehrels 2009, 2010) and a rapidly spinning magnetar (A. Rowlinson et al. 2010, 2013, 2014; S. Dall'Osso et al. 2011; P. T. O'Brien & A. Rowlinson 2012; B. P. Gompertz et al. 2015; N. Rea et al. 2015; G. Stratta et al. 2018). In addition, researchers added a third parameter, the peak luminosity of the prompt phase $L_{\rm peak}$, and found that the correlation among the three parameters is stronger (M. G. Dainotti et al. 2016, 2017, 2020a; G. P. Srinivasaragavan et al. 2020; S. Cao et al. 2022).

In the framework of the central engine of a rapidly spinning magnetar, the shallow decay segment is interpreted as the spin-down mechanism (E. Troja et al. 2007; N. Lyons et al. 2010; A. Rowlinson et al. 2010, 2013; H.-J. Lü & B. Zhang 2014; H.-J. Lü et al. 2015; M. De Pasquale et al. 2016; Q. Zhang et al. 2016; N. Sarin et al. 2020). After a rapidly rotating magnetar loses a significant portion of its rotational energy through the spin-down mechanism, and the centrifugal force can no longer support gravity, the magnetar would collapse into a BH. In this scenario, due to the sudden cessation of activity of the magnetar's center engine, the X-ray shallow decay emission suddenly stops, and a steep decay segment follows the end of the shallow decay segment.

However, the shallow decay segment of most long bursts does not follow the steep decay segment (P. T. O'Brien et al. 2006; E.-W. Liang et al. 2007; T. Sakamoto et al. 2007; R. Willingale et al. 2007, 2010; B. Zhang et al. 2007; M. G. Dainotti et al. 2008, 2010, 2011, 2013, 2017, 2020a; L. Zhao et al. 2019).

Therefore, the shallow decay segment of these bursts may not be produced by the spin-down mechanism of a magnetar. The central engine of these bursts may be a hyperaccreting BH system. In general, the progenitors of long GRBs have a core–envelope structure. The hyperaccreting BH system could power the prompt phase and the early afterglow phase of a GRB through the accretion of the progenitor core materials (P. Kumar et al. 2008; J. K. Cannizzo & N. Gehrels 2009, 2010). In the later period, the hyperaccreting BH system accretes progenitor envelope material and launches a relativistic jet (X.-F. Wu et al. 2013; Y. B. Yu et al. 2015; H. Gao et al. 2016b). The jet could be continuously injected into the afterglow blast wave and may produce a shallow decay segment through external dissipation mechanisms. We refer to this model as the fallback accretion energy external dissipation model.

Up to now, L. Zhao et al. (2020) have successfully interpreted the second plateau of three long GRBs by using the fallback accretion energy external dissipation model within the central engine of a rapidly spinning magnetar. In this paper, we will study the shallow decay segment by using the fallback accretion energy external dissipation model within the framework of a BH central engine. Data reduction and sample selection are described in Section 2. We present the fallback accretion energy external dissipation model in Section 3. In Section 4, we apply the fallback accretion energy external dissipation model to the shallow decay segment in our sample. In Section 5, we test whether the progenitor of the GRB can provide enough envelope material to satisfy the accretion of the BH. Finally, we analyze and summarize our results in Section 6. Throughout the paper, the convention $Q = 10^n Q_n$ is adopted in c.g.s. units.

2. Data Reduction and Sample Selection

Several studies have investigated the shallow decay segment based on Swift/XRT data between 2004 February and 2019 August (E.-W. Liang et al. 2007; M. G. Dainotti et al. 2008, 2010, 2013, 2015, 2017, 2020a, 2020b; R. Del Vecchio et al. 2016; L. Zhao et al. 2019; G. P. Srinivasaragavan et al. 2020; S. Cao et al. 2022). As of 2023 June, approximately four years have passed, so it is necessary to update the sample of the shallow decay segment. We downloaded the XRT light-curve data of all GRBs detected between 2019 September and 2023 June from the Swift/XRT team website[1] (V. Belokurov et al. 2009), which includes 259 GRBs, and processed them with the software HEASOFT(v6.12) (Nasa High Energy Astrophysics Science Archive Research Center (Heasarc) 2014). HEASOFT is a software package that combines XANADU and FTOOLS software packages. XANADU is used for high-level and multitask analysis of X-ray spectra, light curves, and imaging data. FTOOLS software is a specialized tool for processing FITS files. We visually identified the candidates with a shallow decay segment and determined the start time (t_1) of this segment and the end time (t_2) of the follow-up segment. A total of 19 candidates were selected. Next, we used a smooth broken power-law (BPL) function to fit the light curve of these candidates in the interval [t_1, t_2]:

$$f(t) = f_0\left[\left(\frac{t}{t_b}\right)^{w\alpha_1} + \left(\frac{t}{t_b}\right)^{w\alpha_2}\right]^{-1/w}. \quad (1)$$

Here α_1 and α_2 represent the decay scopes of the pre-break and post-break segments, respectively. w describes the sharpness of the break, and we set $w = 3$ as adopted by E.-W. Liang et al. (2007) and L. Zhao et al. (2019).

Based on the fitting results, we formulated the selection criteria and further selected the sample with a shallow decay segment from the candidates. The selection criteria are as follows: (1) since we are studying long bursts, the prompt emission duration T_{90} of the GRB needs to satisfy $T_{90} > 2$ s; (2) the GRB has a redshift measurement; (3) the decay scope of the shallow decay segment should satisfy $\alpha_1 < 0.65$[2]; (4) the decay scope of follow-up segment should be $\alpha_2 < 3$, otherwise the shallow decay segment should be classified as "internal X-ray plateaus." The central engine of GRBs with "internal X-ray plateaus" is likely to be a rapidly spinning magnetar rather than a hyperaccreting BH system (E. Troja et al. 2007; N. Lyons et al. 2010; A. Rowlinson et al. 2010, 2013; H.-J. Lü & B. Zhang 2014; H.-J. Lü et al. 2015; M. De Pasquale et al. 2016; Q. Zhang et al. 2016; N. Sarin et al. 2020). Through the above selection criteria, we selected five GRBs from the candidates. Additionally, we applied the selection criteria to the samples of E.-W. Liang et al. (2007), L. Zhao et al. (2019), and S. Cao et al. (2022) and selected another 98 GRBs. The fitting results of these GRBs' shallow decay segments and follow-up segments based on a BPL function are shown in Figure 1. The name of those GRBs, some Burst Alert Telescope (BAT) observation properties (including T_{90}, the power-law index of the time-averaged spectrum Γ_γ, and the fluence in the 15–150–keV band S_γ), redshift, and the fit result of the shallow decay segment with follow-up segment are listed in Table 1. For the total sample, T_{90}, Γ_γ, S_γ, z, t_1, t_2, t_b, α_1, and α_2 are distributed in the ranges 2.4–549.9 s, 0.66–2.9, 0.74–409 $\times$ 10^{-7} erg cm^{-2}, 0.037–6, 19.51–2.82 $\times$ 10^4 s, 1.66 $\times$ 10^4–1.26 $\times$ 10^7 s, 2.40 $\times$ 10^2–3.31 $\times$ 10^5 s, −0.55–0.64, and 0.85–2.46, respectively. In addition, the average values of these parameter distributions are 82.04 s, 1.70, 44.14 $\times$ 10^{-7} erg cm^{-2}, 2.08, 4.17 $\times$ 10^2 s, 5.75 $\times$ 10^5 s, 8.71 $\times$ 10^3 s, 0.32, and 1.43, respectively.

3. Model Application

Systematic analysis of GRBs suggests that long bursts may be related to the death of massive stars (S. E. Woosley 1993; B. Paczyński 1998; A. I. MacFadyen & S. E. Woosley 1999; S. E. Woosley & J. S. Bloom 2006). The progenitors of GRBs generally have a core–envelope structure, which is a common stellar model. When the progenitor star is at the end of its evolution, electron capture and photon decomposition can trigger core collapse. The progenitor material will then fall back to the equatorial plane. Most of the core material does not have enough centrifugal force to support itself and thus directly forms an initial BH. The fallback radius of the remaining material is greater than the radius of the BH's innermost stable circular orbit $R_{\rm isco}$, and this material will enter an orbit around the BH to form an accretion disk, thus forming a hyperaccreting BH system

[1] http://www.swift.ac.uk/xrt_curves/

[2] The selection criteria adopted by E.-W. Liang et al. (2007) and L. Zhao et al. (2019) in their studies of the shallow decay segment were $\alpha_1 < 0.75$ and $\alpha_1 < 0.8$, respectively. In addition, L. Zhao et al. (2019), based on the Swift/XRT data between 2004 February and 2017 July, found that α_1 fits the normal distribution with $\alpha_1 = 0.43 \pm 0.22$. We have tested that adjusting the standard values 0.75, 0.8, and 0.65 (the upper limit of the distribution) reasonably may slightly change the size of the final sample, but it will not affect the main conclusion. In this paper, we adopt the selection criterion $\alpha_1 < 0.65$.

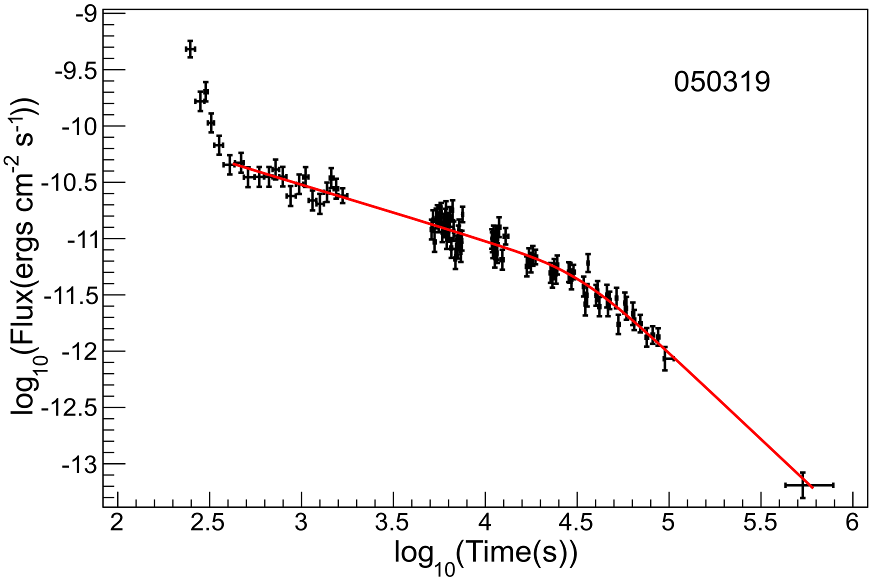

Figure 1. The fitting results of shallow decay segments and follow-up segments in our sample based on a BPL function.
(The complete figure set (103 images) is available in the online article.)

(P. Kumar et al. 2008; J. K. Cannizzo & N. Gehrels 2009, 2010). The hyperaccreting BH system can launch a relativistic jet through either the neutrino-annihilation mechanism (R. Popham et al. 1999; R. Narayan et al. 2001; T. Di Matteo et al. 2002; A. Janiuk et al. 2004; W.-M. Gu et al. 2006; W.-X. Chen & A. M. Beloborodov 2007; T. Liu et al. 2007, 2015; W. H. Lei et al. 2009; W.-H. Lei et al. 2017; W. Xie et al. 2016) or the Blandford–Znajek (BZ) mechanism (R. D. Blandford & R. L. Znajek 1977; H. K. Lee et al. 2000; L.-X. Li 2000; W.-H. Lei et al. 2005, 2013). The relativistic jet successfully penetrates the stellar envelope material, powering the the prompt emission of the GRB through internal dissipation and contributing to multiband afterglow emission through external shocks (especially a forward shock) generated by interactions with the surrounding medium (B. Zhang 2018). During the penetration process of the jet, some of the jet energy is transferred to the envelope material, which may contribute to the explosion of a supernova. The shock generated by a supernova explosion will transfer kinetic energy to the envelope material, causing some of it to be ejected. The rest of the envelope material will fall back to the BH in the late stage to form a new accretion disk with a larger radius, reactivating the BH's accretion mechanism. Under the central engine of the hyperaccreting BH system, both the neutrino-annihilation mechanism and the BZ mechanism can extract the rotational energy of the BH and launch a relativistic jet. The difference is that the BZ mechanism launches a jet dominated by the Poynting flux, while the neutrino-annihilation mechanism launches a hot fireball. Compared to the neutrino-annihilation mechanism, the BZ mechanism launches cleaner and more energetic jets, which may describe the activity of the central engine in the late stage of GRBs (N. Kawanaka et al. 2013; W.-H. Lei et al. 2017; W. Xie et al. 2017; N. M. Lloyd-Ronning et al. 2018). Some of the BZ energy is internally dissipated, while the rest is injected into the relatively low-velocity blast wave of the GRB afterglow. If the injected energy is equal to or even greater than the kinetic energy of the blast wave, the blast wave will form an extremely relativistic shock when sweeping through the interstellar medium, generating a magnetic field in the process. Electrons will lose energy through synchrotron radiation, potentially producing a shallow decay segment.

3.1. Fallback Accretion Model

During the collapse process of the progenitor star, most of the material in the core will not have sufficient centrifugal force to support it, thus directly forming a BH. The envelope material will fall back around the BH in the later stage to form a new accretion disk. The fallback rate on the new accretion disk should be equivalent to the mass loss rate of the progenitor star, which can be described by a BPL function (R. A. Chevalier 1989; A. I. MacFadyen et al. 2001; W. Zhang et al. 2008; Z. G. Dai & R.-Y. Liu 2012):

$$\dot{M}_{\rm fb} = \dot{M}_p \left[\frac{1}{2}\left(\frac{t - t_0}{t_p - t_0}\right)^{-s/2} + \frac{1}{2}\left(\frac{t - t_0}{t_p - t_0}\right)^{5s/3} \right]^{-1/s}, \quad (2)$$

where t_0 is the starting time of the fallback accretion in the cosmologically local frame, and $\dot{M}_p$ and t_p are the peak rate and the peak time in the fallback process, respectively.

The material from the progenitor star will fall back and form an accretion disk, which will be accreted by the BH in a viscous manner. The accretion rate can be expressed as (P. Kumar et al. 2008; P. Kumar & J. L. Johnson 2010)

$$\dot{M} = \frac{M_d}{\tau_{\rm vis}}. \quad (3)$$

In the above equation, $\tau_{\rm vis}$ represents the viscosity time of accretion disks, which can be estimated as

$$\tau_{\rm vis} \sim \frac{r_d^2}{\nu(r_d)} \quad (4)$$

where $\nu(r_d)$ is kinematic coefficient of viscosity for a thick disk with vertical scale height r_d.

The mass of the accretion disk M_d increases with the fallback process and decreases with the accretion process, therefore (P. Kumar et al. 2008; P. Kumar & J. L. Johnson 2010;

Table 1
Features of the Sample

GRB Name	T_{90} (s)	Γ_γ	S_γ (10^{-7} erg cm^{-2})	References[a]	z	References[b]	$\log_{10}(t_1)$ (s)	$\log_{10}(t_2)$ (s)	$\log_{10}(t_b)$ (s)	α_1	α_2
050319	10 ± 2	8 ± 0.8	2.2 ± 0.2	3119	3.24	3136	2.61	5.74	4.52	0.51 ± 0.03	1.54 ± 0.11
050401	33 ± 2	1.5 ± 0.06	140 ± 14	3173	2.9	3176	2.1	5.91	3.67	0.55 ± 0.02	1.43 ± 0.04
050416A	2.4 ± 0.2	2.9 ± 0.2	69	3273	0.6528	3542	2.26	6.77	3.22	0.39 ± 0.1	0.9 ± 0.02
050714B	46.7	2.6 ± 0.3	6.5 ± 1.4	3615	2.438	B07	3.75	5.89	4.56	0.22 ± 0.29	0.85
050802	13 ± 2	1.6 ± 0.1	28 ± 3	3737	1.7102	3749	2.89	6.08	3.72	0.48 ± 0.07	1.56 ± 0.02
050822	102 ± 2	2.5 ± 0.1	34 ± 3	3856	1.434	H12	3.02	6.66	4.27	0.29 ± 0.07	1.08 ± 0.03
050824	25 ± 5	2.7 ± 0.4	2.8 ± 0.5	3871	0.8278	3874	3.75	6.41	4.82	0.24 ± 0.1	0.93 ± 0.08
050826	35 ± 8	1.2 ± 0.3	4.3 ± 0.7	3888	0.296	5982	4.03	5.1	4.61	0.27 ± 0.33	1.96 ± 0.71
051221A	1.4	1.08 ± 0.14	32 ± 1	4363, 4394	0.5465	4384	2.86	6.03	4.63	0.56 ± 0.04	1.43 ± 0.07
060108	14.4 ± 1	2.01 ± 0.17	3.7 ± 0.4	4445	2.03	4539	2.66	5.57	4.11	0.26 ± 0.06	1.25 ± 0.08
060115	142 ± 5	1.76 ± 0.12	19 ± 1	4518	3.5328	4520	2.9	5.62	4.5	0.62 ± 0.05	1.2 ± 0.12
060306	61 ± 2	1.85 ± 0.1	22 ± 1	4851	1.55	P13	2.57	5.58	3.51	0.31 ± 0.14	1.06 ± 0.03
060502A	33 ± 5	1.43 ± 0.08	22 ± 1	5053	1.5026	5052	2.35	6.2	4.57	0.59 ± 0.03	1.18 ± 0.05
060604	10 ± 3	1.9 ± 0.41	1.3 ± 0.3	5214	2.1357	5218	3.56	6.2	4.32	0.39 ± 0.09	1.29 ± 0.06
060605	15 ± 2	1.34 ± 0.15	4.6 ± 0.4	5231	3.773	5226	2.24	5.25	3.92	0.42 ± 0.03	2.06 ± 0.08
060614	102	1.57 ± 0.12	409 ± 18	5264	0.1257	5276	3.66	6.4	4.69	0.09 ± 0.04	1.94 ± 0.04
060707	68 ± 5	0.66 ± 0.63	17 ± 2	5289	3.4240	5298	2.58	6.53	5.09	0.62 ± 0.03	1.32 ± 0.12
060714	115 ± 5	1.99 ± 0.1	30 ± 2	5334	2.7108	5320	2.47	6.11	3.67	0.38 ± 0.09	1.27 ± 0.04
060719	55 ± 5	2 ± 0.11	16 ± 1	5349	1.5320	K12	2.71	5.88	3.87	0.48 ± 0.07	1.25 ± 0.04
060729	116 ± 10	1.86 ± 0.14	27 ± 2	5370	0.5428	F09	2.83	7.1	4.8	0.12 ± 0.02	1.37 ± 0.01
060805A	5.4 ± 0.5	2.23 ± 0.42	0.74 ± 0.2	5403	2.44	P09	2.16	5.46	3.56	0.19 ± 0.17	1.5 ± 0.1
060814	134 ± 4	1.43 ± 0.16	269 ± 12	5460	1.9229	K12	3.15	6.12	4.1	0.44 ± 0.08	1.36 ± 0.03
060906	43.6 ± 1	2.02 ± 0.11	22.1 ± 1.4	5534, 5538	3.6856	5535	2.8	5.41	4.05	0.24 ± 0.06	1.74 ± 0.09
060908	19.3 ± 0.3	1.33 ± 0.07	29 ± 1	5551	1.8836	F09	1.8	5.94	2.84	0.56 ± 0.07	1.44 ± 0.04
061121	81 ± 5	1.32 ± 0.05	137 ± 2	5831, 5837	1.3145	5826	2.37	6.32	3.71	0.36 ± 0.03	1.4 ± 0.02
070103	19 ± 1	2 ± 0.2	3.4 ± 0.5	5991	2.6208	K12	2.2	5.13	3.16	-0.23 ± 0.14	1.42 ± 0.06
070129	460 ± 20	2.05 ± 0.16	31 ± 3	6058	2.3384	K12	3.15	6.21	4.25	0.15 ± 0.08	1.14 ± 0.03
070306	209.5 ± 10	1.72 ± 0.1	53.80 ± 2.86	6173	1.49594	6202	2.73	6.05	4.48	0.11 ± 0.03	1.81 ± 0.04
070508	21 ± 1	0.81 ± 0.07	196 ± 2.73	6390, 6403	0.82	6398	1.83	5.9	2.46	0.18 ± 0.32	0.95 ± 0.18
070521	37.9 ± 2	1.10 ± 0.17	80 ± 2	6440	0.553	C22	1.51	5.73	3.35	0.19 ± 0.11	1.56 ± 0.03
070529	109.2 ± 3	1.38 ± 0.16	25.70 ± 2.45	6468	2.4996	6470	2.31	5.78	3.02	0.48 ± 0.16	1.25 ± 0.04
070810A	11 ± 1	2.04 ± 0.14	6.9 ± 0.6	6748	2.17	6741	2.1	4.54	3.14	0.36 ± 0.25	1.32 ± 0.06
080310	365 ± 20	2.32 ± 0.16	23 ± 2	7402	2.42	7389	2.03	6.04	4.03	0.25 ± 0.06	1.55 ± 0.05
080413B	8 ± 1	1.26 ± 0.27	32 ± 1	7606	1.1014	7601	2.1	5.24	2.6	0.38 ± 0.12	1 ± 0.01
080430	16.2 ± 2.4	1.73 ± 0.09	12 ± 1	7656	0.767	7654	2.5	6.48	4.53	0.43 ± 0.02	1.16 ± 0.03
080516	5.8 ± 0.3	1.82 ± 0.27	2.6 ± 0.4	7736	3.2	7747	2.1	4.67	3.67	0.33 ± 0.09	1.07 ± 0.11
080707	27.1 ± 1.1	1.77 ± 0.19	5.2 ± 0.6	7953	1.2322	7949	2.4	5.45	4.03	0.28 ± 0.07	1.17 ± 0.1
080905B	128 ± 16	1.78 ± 0.15	18 ± 2	8188	2.3739	8191	2.27	4.75	4.16	0.47 ± 0.02	2.18
081029	270 ± 45	1.43 ± 0.18	21 ± 2	8447	3.8479	8438	3.4	5.84	4.21	0.43 ± 0.05	2.46 ± 0.09
081221	34 ± 1	1.21 ± 0.13	181 ± 3	8708	2.26	C22	2.31	5.98	2.76	0.27 ± 0.08	1.29 ± 0.01
090113	9.1 ± 0.9	1.6 ± 0.1	7.6 ± 0.4	8808	1.7493	K12	2	5.52	2.75	0.13 ± 0.16	1.29 ± 0.04
090205	8.8 ± 1.8	2.15 ± 0.23	1.9 ± 0.3	8886	4.6497	8892	2.63	5.53	4.18	0.54 ± 0.06	1.98 ± 0.23
090313	78 ± 19	1.91 ± 0.29	14 ± 2	8986	3.375	8994	4.45	5.86	4.89	0.6 ± 0.18	2.3 ± 0.12
090404	84 ± 14	2.32 ± 0.08	30 ± 1	9089	3	P13	2.49	6.16	4.23	0.20 ± 0.07	1.25 ± 0.06
090407	310 ± 70	1.73 ± 0.29	11 ± 2	9104	1.4485	K12	3.07	6.05	4.86	0.38 ± 0.03	1.67 ± 0.09
090418A	56 ± 5	1.48 ± 0.07	46 ± 2	9157	1.608	9151	2.09	5.64	3.49	0.47 ± 0.05	1.58 ± 0.04
090424	52	0.9 ± 0.02	201	9230	0.544	9243	2.43	6.70	2.97	0.57 ± 0.17	1.17 ± 0.02

Table 1
(Continued)

GRB Name	T_{90} (s)	Γ_γ	S_γ (10^{-7} erg cm^{-2})	References[a]	z	References[b]	$\log_{10}(t_1)$ (s)	$\log_{10}(t_2)$ (s)	$\log_{10}(t_b)$ (s)	α_1	α_2
090529	100	2 ± 0.3	6.8 ± 1.7	9434	2.625	9457	3.41	5.89	5.36	0.51 ± 0.1	1.69 ± 0.43
090530	48 ± 36	1.61 ± 0.17	11 ± 1	9443	1.266	15571	2.2	5.90	4.77	0.61 ± 0.02	1.35 ± 0.1
091018	4.4 ± 0.6	1.77 ± 0.24	14 ± 1	10040	0.971	10038	1.7	5.9	2.78	0.43 ± 0.05	1.2 ± 0.02
091029	39.2 ± 5	1.46 ± 0.27	24 ± 1	10103	2.752	10100	2.86	6.28	4.07	0.19 ± 0.04	1.15 ± 0.02
100302A	17.9 ± 1.7	1.72 ± 0.19	3.1 ± 0.4	10462	4.813	10466	3.10	6.04	4.35	0.35 ± 0.12	0.95 ± 0.08
100418A	7 ± 1	2.16 ± 0.25	3.4 ± 0.5	10615	0.6235	10620	3	6.47	4.91	-0.16 ± 0.06	1.44 ± 0.08
100425A	37 ± 2.4	2.42 ± 0.32	4.7 ± 0.9	10685	1.755	10684	2.53	5.7	4.51	0.54 ± 0.05	1.2 ± 0.13
100901A	439 ± 33	1.59 ± 0.21	21 ± 3	11169	1.408	11164	3.59	5.98	4.58	-0.02 ± 0.03	1.5 ± 0.03
110106B	24.8 ± 4.8	1.76 ± 0.11	20 ± 1	11533	0.618	11538	2.5	5.73	4.12	0.58 ± 0.05	1.41 ± 0.07
110213A	48 ± 16	1.83 ± 0.12	59 ± 4	11714	1.46	11708	2.21	5.98	3.53	0.02 ± 0.03	1.82 ± 0.02
110808A	48 ± 23	2.32 ± 0.43	3.3 ± 0.8	12262	1.348	12258	2.69	5.79	5.22	0.57 ± 0.05	1.41 ± 0.41
111008A	63.46 ± 2.19	1.86 ± 0.09	53 ± 3	12424	4.9898	12431	2.47	6.01	3.9	0.32 ± 0.04	1.31 ± 0.03
111228A	101.2 ± 5.42	2.27 ± 0.06	85 ± 2	12749	0.716	12761	2.62	6.47	4.13	0.4 ± 0.03	1.27 ± 0.02
120118B	23.26 ± 4.02	2.08 ± 0.11	18 ± 1	12873	2.943	14225	2.61	5.53	3.33	-0.55 ± 0.18	1.03 ± 0.06
120326A	69.6 ± 8.3	1.41 ± 0.34	26 ± 3	13120	1.798	13118	3.01	6.21	4.71	-0.24 ± 0.02	2.04 ± 0.06
120404A	38.7 ± 4.1	1.85 ± 0.13	16 ± 1	13220	2.88	13227	2.61	5.37	3.69	0.54 ± 0.13	1.96 ± 0.12
120521C	26.7 ± 4.4	1.73 ± 0.11	11 ± 1	13333	6	13348	2.75	5.15	4.06	0.35 ± 0.14	1.1 ± 0.2
120811C	26.8 ± 3.7	1.4 ± 0.3	30 ± 3	13634	2.671	13628	2.4	5	3.34	0.43 ± 0.11	1.12 ± 0.08
120907A	16.9 ± 8.9	1.73 ± 0.25	6.7 ± 1.1	13720	0.97	13723	1.75	5.45	3.2	0.43 ± 0.07	1.08 ± 0.03
121128A	23.3 ± 1.6	1.32 ± 0.18	69 ± 4	14011	2.2	14009	2.13	5.19	3.2	0.55 ± 0.04	1.63 ± 0.04
131105A	112.3 ± 4.1	1.45 ± 0.11	71 ± 5	15459	1.686	15450	2.61	5.87	3.66	0.16 ± 0.11	1.19 ± 0.04
140206A	93.6 ± 13.8	1.04 ± 0.15	160 ± 3	15805	2.74	15802	2.65	6.23	3.93	0.64 ± 0.02	1.33 ± 0.02
140430A	173.6 ± 3.7	2 ± 0.22	11 ± 2	16200	1.6	16194	2.66	5.66	4.68	0.6 ± 0.09	1.53 ± 0.04
140509A	23.20 ± 5.17	1.59 ± 0.20	12 ± 2	16240	2.4	C22	3.62	5.13	4.08	0.44 ± 0.61	2.04 ± 0.18
140518A	60.5 ± 2.4	0.92 ± 0.61	10 ± 1	16306	4.707	16301	2.8	4.27	3.28	-0.16 ± 0.31	1.38 ± 0.2
140703A	67.1 ± 67.9	1.74 ± 0.13	39 ± 3	16509	3.14	16505	2.34	5.48	4.16	0.62 ± 0.03	2.16 ± 0.09
141121A	549.9 ± 37.4	1.73 ± 0.13	53 ± 4	17083	1.47	17081	4.45	6.17	5.52	0.46 ± 0.1	2.24 ± 0.18
150314A	14.79 ± 2.64	1.08 ± 0.03	220 ± 3	17581	1.758	17583	3.56	6.03	3.98	0.25 ± 0.1	1.86 ± 0.04
150323A	149.6 ± 8.9	1.85 ± 0.07	61 ± 2	17628	0.593	17616	2.65	5.58	4.16	0.43 ± 0.05	1.26 ± 0.09
150403A	40.9 ± 11.72	1.23 ± 0.04	170 ± 3	17675	2.06	17672	1.81	6.53	3.33	0.49 ± 0.01	1.34 ± 0.01
150910A	112.2 ± 38.3	1.42 ± 0.12	48 ± 4	18268	1.359	18273	3.03	5.5	3.94	0.61 ± 0.14	2.36 ± 0.16
151027A	129.69 ± 5.55	1.72 ± 0.05	78 ± 2	18496	0.81	18487	2.71	6.1	3.6	0.06 ± 0.03	1.65 ± 0.02
151112A	19.32 ± 31.24	1.77 ± 0.21	9.4 ± 1.2	18593	4.1	18603	3.63	5.83	4.76	0.64 ± 0.08	1.6 ± 0.25
160121A	12.0 ± 2.4	1.77 ± 0.13	6.1 ± 0.5	18919	1.645	18925	2.51	4.83	4.22	0.27 ± 0.05	1.50 ± 0.39
160227A	316.5 ± 75.4	0.75 ± 0.51	31 ± 2	19106	2.38	19109	3.2	6.4	4.37	0.28 ± 0.09	1.2 ± 0.04
160327A	28 ± 9	1.84 ± 0.11	14 ± 1	19240	4.99	19245	2.53	5	3.62	0.3 ± 0.14	1.56 ± 0.09
160804A	144.2 ± 19.2	1.4 ± 0.23	114 ± 3	19765	0.736	19773	3.02	6.13	3.96	-0.28 ± 0.27	0.92 ± 0.05
161108A	105.1 ± 11.9	1.85 ± 0.17	11 ± 1	20151	1.159	20150	2.81	5.96	4.36	-0.02 ± 0.16	0.86 ± 0.07
161129A	35.53 ± 2.09	1.57 ± 0.06	36 ± 1	20220	0.645	20245	2.44	4.24	3.56	0.38 ± 0.11	2.18 ± 0.11
170113A	20.66 ± 4.4	0.75 ± 0.59	6.7 ± 0.7	20456	1.968	20458	2.41	5.94	3.64	0.48 ± 0.04	1.25 ± 0.02
170202A	46.2 ± 11.5	1.68 ± 0.07	33 ± 1	20596	3.645	20584	2.47	5.73	3.32	-0.12 ± 0.1	1.15 ± 0.04
170705A	217.3 ± 18	1.65 ± 0.05	95 ± 3	21296	2.01	21298	2.74	6.45	4.16	0.45 ± 0.03	1.12 ± 0.02
170903A	29.2 ± 4.4	1.94 ± 0.12	24 ± 2	21796	0.886	21799	3.51	6.01	4.06	0.03 ± 0.22	0.99 ± 0.05
171222A	174.8 ± 22.7	2.07 ± 0.17	19 ± 2	22280	2.409	22272	3.52	6.01	4.92	0.22 ± 0.13	0.98 ± 0.18
180115A	40.9 ± 3.0	1.66 ± 0.22	7.6 ± 1.1	22348	2.487	22346	2.71	5.52	4.06	0.64 ± 0.05	1.47 ± 0.08
180329B	210 ± 44	0.97 ± 0.56	33 ± 3	22566	1.998	C22	2.74	5.32	3.85	0.31 ± 0.06	1.57 ± 0.07
180404A	35.2 ± 5.3	1.95 ± 0.12	13 ± 1	22599	1	22591	2.50	5.52	4.26	0.24 ± 0.04	1.48 ± 0.11

Table 1
(Continued)

GRB Name	T_{90} (s)	Γ_γ	S_γ (10^{-7} erg cm^{-2})	References[a]	z	References[b]	$\log_{10}(t_1)$ (s)	$\log_{10}(t_2)$ (s)	$\log_{10}(t_b)$ (s)	α_1	α_2
180620B	198.8 ± 27.4	1.60 ± 0.05	100 ± 3	22821	1.1175	22823	3.51	6.12	4.38	0.47 ± 0.19	0.99 ± 0.09
181010A	16.4 ± 2.2	1.52 ± 0.15	6.9 ± 0.7	23321	1.39	23315	1.91	5.79	3.21	0.52 ± 0.07	1.07 ± 0.03
190106A	76.8 ± 2.4	1.34 ± 0.21	60 ± 2	23625	1.86	23632	2.49	6.13	4.24	0.35 ± 0.03	1.35 ± 0.03
190114A	66.6 ± 10.2	2.06 ± 0.22	8 ± 1.2	23685	3.3765	23680	2.51	4.83	3.35	-0.18 ± 0.14	1.20 ± 0.05
201221A	44.5 ± 6.2	1.40 ± 0.15	19 ± 2	29116	5.7	29110	2.63	5.01	4.11	0.46 ± 0.07	1.99 ± 0.14
210104A	32.06 ± 0.49	1.55 ± 0.14	88 ± 2	29251	0.46	Z22	2.03	5.51	2.89	0.17 ± 0.03	1.19 ± 0.01
210210A	6.6 ± 0.59	2.46 ± 0.12	9.8 ± 0.8	29467	0.715	29450	1.52	5.49	3.62	0.29 ± 0.04	1.68 ± 0.07
210610A	13.62 ± 3.15	1.41 ± 0.19	10 ± 1	30186	3.54	30164	1.81	5.57	3.06	0.11 ± 0.09	1.05 ± 0.06
230325A	38.05 ± 11.56	1.82 ± 0.18	13 ± 2	33523	1.664	33521	3.01	5.98	4.91	0.43 ± 0.09	1.23 ± 0.15

Notes.
[a] The references of GRB prompt phase observations for our sample.
[b] The references of GRB redshift for our sample.

References. (B07) N. R. Butler (2007); (C22) S. Cao et al. (2022); (F09) J. P. U. Fynbo et al. (2009); (H12) J. Hjorth et al. (2012); (K12) T. Krühler et al. (2012); (P13) D. A. Perley et al. (2013); (Z22) L.-L. Zhang et al. (2022); (3119) H. Krimm et al. (2005a); (3136) J. P. U. Fynbo et al. (2005a); (3173) T. Sakamoto et al. (2005a); (3176) J. P. U. Fynbo et al. (2005b); (3273) T. Sakamoto et al. (2005b); (3542) S. B. Cenko et al. (2005); (3615) J. Tueller et al. (2005); (3737) D. Palmer et al. (2005); (3749) J. P. U. Fynbo et al. (2005c); (3856) D. Hullinger et al. (2005); (3871) H. Krimm et al. (2005b); (3874) J. P. U. Fynbo et al. (2005d); (3888) C. Markwardt et al. (2005); (4363) A. Parsons et al. (2005); (4384) E. Berger & A. M. Soderberg (2005); (4394) S. Golenetskii et al. (2005); (4445) T. Sakamoto et al. (2006a); (4518) L. Barbier et al. (2006a); (4520) S. Piranomonte et al. (2006); (4539) A. Melandri et al. (2006); (4851) D. Hullinger et al. (2006); (5052) A. Cucchiara et al. (2006); (5053) A. Parsons et al. (2006a); (5214) A. Parsons et al. (2006b); (5218) A. J. Castro-Tirado et al. (2006); (5226) A. Still et al. (2006); (5231) G. Sato et al. (2006a); (5264) S. Golenetskii et al. (2006a); (5276) D. Fugazza et al. (2006); (5289) M. Stamatikos et al. (2006); (5298) P. Jakobsson et al. (2006a); (5320) P. Jakobsson et al. (2006b); (5334) H. Krimm et al. (2006c); (5349) T. Sakamoto et al. (2006b); (5370) A. Parsons et al. (2006c); (5403) L. Barbier et al. (2006b); (5460) S. Golenetskii et al. (2006b); (5534) T. Sakamoto et al. (2006c); (5535) P. Vreeswijk et al. (2006); (5538) G. Sato et al. (2006b); (5551) D. Palmer et al. (2006); (5826) J. S. Bloom et al. (2006); (5831) E. Fenimore et al. (2006); (5837) S. Golenetskii et al. (2006c); (5982) J. P. Halpern & Mirabal (2006); (5991) L. Barbier et al. (2007); (6058) H. Krimm et al. (2007); (6173) S. D. Barthelmy et al. (2007a); (6202) A. O. Jaunsen et al. (2007b); (6390) S. D. Barthelmy et al. (2007b); (6398) P. Jakobsson et al. (2007); (6403) S. Golenetskii et al. (2007); (6440) D. Palmer et al. (2007); (6468) A. Parsons et al. (2007); (6470) E. Berger et al. (2007); (6741) C. C. Thoene et al. (2007); (6748) C. Markwardt et al. (2007); (7389) E. Berger & M. Rauch (2008); (7402) J. Tueller et al. (2008); (7601) P. M. Vreeswijk et al. (2008a); (7606) S. D. Barthelmy et al. (2008a); (7654) A. Cucchiara & D. B. Fox (2008); (7656) M. Stamatikos et al. (2008); (7736) H. Krimm et al. (2008); (7747) R. Filgas et al. (2008); (7949) J. P. U. Fynbo et al. (2008); (7953) P. Schady & F. E. Marshall (2008); (8188) S. D. Barthelmy et al. (2008b); (8191) P. M.Vreeswijk et al. (2008b); (8438) V. D'Elia et al. (2008); (8447) J. R. Cummings et al. (2008b); (8708) J. R. Cummings et al. (2008a); (8808) J. Tueller et al. (2009a); (8886) J. R. Cummings et al. (2009); (8892) D. Fugazza et al. (2009); (8986) T. Sakamoto et al. (2009); (8994) R. Chornock et al. (2009); (9089) J. Tueller et al. (2009b); (9104) T. N. Ukwatta et al. (2009); (9151) R. Chornock et al. (2009a); (9157) E. E. Fenimore et al. (2009); (9230) V. Connaughton (2009); (9243) R. Chornock et al. (2009b); (9434) C. B. Markwardt et al. (2009a); (9443) D. M. Palmer et al. (2009); (9457) D. Malesani et al. (2009); (10038) H.-W. Chen et al. (2009); (10040) C. B. Markwardt et al. (2009b); (10100) R. Chornock et al. (2009c); (10103) S. D. Barthelmy et al. (2009); (10462) J. R. Cummings et al. (2010); (10466) R. Chornock et al. (2010a); (10615) T. N. Ukwatta et al. (2010); (10620) L. A. Antonelli et al. (2010); (10684) P. Goldoni et al. (2010); (10685) C. B. Markwardt et al. (2010); (11164) R. Chornock et al. (2010b); (11169) T. Sakamoto et al. (2010); (11533) T. N. Ukwatta et al. (2011); (11538) R. Chornock et al. (2011); (11708) P. A. Milne & S. B. Cenko (2011); (11714) S. D. Barthelmy et al. (2011); (12258) A. de Ugarte Postigo et al. (2011); (12262) T. Sakamoto et al. (2011); (12424) W. H. Baumgartner et al. (2011); (12431) K. Wiersema et al. (2011); (12749) J. R. Cummings et al. (2011); (12761) A. Cucchiara & A. J. Levan (2011); (12873) T. Sakamoto et al. (2012); (13118) J. C. Tello et al. (2012); (13120) S. D. Barthelmy et al. (2012); (13227) V. D'Elia et al. (2012); (13220) T. N. Ukwatta et al. (2012); (13333) C. B. Markwardt et al. (2012); (13348) N. R. Tanvir et al. (2012b); (13628) C. C. Thoene et al. (2012); (13634) H. A. Krimm et al. (2012); (13720) M. Stamatikos et al. (2012); (13723) R. Sanchez-Ramirez et al. (2012); (14009) N. R. Tanvir et al. (2012a); (14011) D. M. Palmer et al. (2012); (14225) D. Malesani et al. (2013); (15450) D. Xu et al. (2013); (15459) W. H. Baumgartner et al. (2013); (15571) P. Goldoni et al. (2013); (15802) V. D'Elia et al. (2014); (15805) T. Sakamoto et al. (2014); (16194) T. Kruehler et al. (2014); (16200) H. A. Krimm et al. (2014a); (16240) D. M. Palmer et al. (2014); (16301) R. Chornock et al. (2014); (16306) T. N. Ukwatta et al. (2014); (16505) A. J. Castro-Tirado et al. (2014); (16509) H. A. Krimm et al. (2014b); (17081) D. A. Perley et al. (2014); (17083) H. A. Krimm et al. (2014c); (17583) A. de Ugarte Postigo et al. (2015); (17616) D. A. Perley & S. B. Cenko (2015); (17628) C. B. Markwardt et al. (2015); (17581) J. R. Cummings et al. (2015); (17672) V. Pugliese et al. (2015); (17675) T. Sakamoto et al. (2015); (18268) A. Y. Lien et al. (2015); (18273) W. Zheng et al. (2015); (18487) D. A. Perley et al. (2015); (18496) D. M. Palmer et al. (2015); (18593) H. A. Krimm et al. (2015); (18603) J. Bolmer et al. (2015); (18925) R. Sanchez-Ramirez et al. (2016); (19106) T. Sakamoto et al. (2016); (19109) D. Xu et al. (2016a); (19240) C. B. Markwardt et al. (2016); (19245) A. de Ugarte Postigo et al. (2016a); (19765) H. A. Krimm et al. (2016); (19773) D. Xu et al. (2016b); (20150) de Ugarte Postigo et al. (2016b); (20151) D. M. Palmer et al. (2016); (20220) K. P. Mooley et al. (2016); (20245) Z. Cano et al. (2016); (20456) C. B. Markwardt et al. (2017); (20458) D. Xu et al. (2017); (20584) de Ugarte Postigo et al. (2017a); (20596) S. D. Barthelmy et al. (2017b); (21296) H. A. Krimm et al. (2017); (21298) de Ugarte Postigo et al. (2017d); (21796) S. D. Barthelmy et al. (2017a); (21799) de Ugarte Postigo et al. (2017b); (22272) de Ugarte Postigo et al. (2017c); (22280) D. M. Palmer et al. (2017); (22346) A. de Ugarte Postigo et al. (2018); (22348) S. D. Barthelmy et al. (2018a); (22566) D. M. Palmer et al. (2018); (22591) J. Selsing et al. (2018); (22599) S. D. Barthelmy et al. (2018b); (22821) T. N. Ukwatta et al. (2018); (22823) L. Izzo et al. (2018); (23315) J.-B. Vielfaure et al. (2018); (23321) A. Y. Lien et al. (2018); (23625) D. M. Palmer et al. (2019); (23632) P. Schady et al. (2019); (23680) A. de Ugarte Postigo et al. (2019); (23685) S. D. Barthelmy et al. (2019); (29110) P. Veres & Fermi-GBM Team (2020); (29116) S. D. Barthelmy et al. (2020); (29251) D. M. Palmer et al. (2021); (29450) A. de Ugarte Postigo et al. (2021); (29467) A. Y. Lien et al. (2021); (30164) Z. P. Zhu et al. (2021); (30186) S. D. Barthelmy et al. (2021); (33521) D. Pieterse et al. (2023); (33523) A. Y. Lien et al. (2023).

W.-H. Lei et al. 2017)

$$\dot{M}_d = \dot{M}_{\rm fb} - \dot{M}. \tag{5}$$

By combining Equations (3) and (5), we can derive the accretion rate of the BH (P. Kumar et al. 2008; P. Kumar & J. L. Johnson 2010; W.-H. Lei et al. 2017):

$$\dot{M} = \frac{1}{\tau_{\rm vis}} e^{-t/\tau_{\rm vis}} \int_{t_0}^{t} e^{t'/\tau_{\rm vis}} \dot{M}_{\rm fb} dt'. \tag{6}$$

3.2. BZ Mechanism

The rotational energy extracted by a Kerr BH with a mass of $M_\bullet$ through the BZ mechanism is (H. K. Lee et al. 2000; L.-X. Li 2000; D. X. Wang et al. 2002; W.-H. Lei et al. 2005, 2013, 2017; J. C. McKinney 2005; W.-H. Lei & Zhang 2011; W. Chen et al. 2017; T. Liu et al. 2017; N. M. Lloyd-Ronning et al. 2018)

$$L_{\rm BZ} = 1.7 \times 10^{50} a_\bullet^2 m_\bullet^2 B_{\bullet,15}^2 F(a_\bullet) \ {\rm erg\,s^{-1}}. \tag{7}$$

Here, $m_\bullet = M_\bullet/M_\odot$ is the dimensionless BH mass, $a_\bullet$ is the dimensionless spin of the BH, and $B_{\bullet,15}$ is the strength of the magnetic field threading the BH horizon in units of 10^{15} G. From the above equation, it can be seen that the BZ power mainly depends on $m_\bullet$, $a_\bullet$, and $B_{\bullet,15}$.

$F(a_\bullet)$ in Equation (7) can be written as follows:

$$F(a_\bullet) = \left[\frac{1+q^2}{q^2}\right]\left[\left(q + \frac{1}{q}\right)\arctan q - 1\right], \tag{8}$$

$$q = a_\bullet/(1 + \sqrt{1 - a_\bullet^2}), \tag{9}$$

with

$$a_\bullet = \frac{J_\bullet c}{G M_\bullet^2}, \tag{10}$$

where $J_\bullet$ is the angular momentum of the BH.

The BZ process extracts rotational energy and angular momentum from the BH, while the accretion process brings the energy and angular momentum of the accretion disk into the BH. According to the conservation of energy and angular momentum, the evolution equations of a BH under these two processes are as follows (D. X. Wang et al. 2002):

$$\frac{dM_\bullet c^2}{dt} = \dot{M} c^2 E_{\rm in} - P_{\rm BZ}, \tag{11}$$

$$\frac{dJ_\bullet}{dt} = L_{\rm in}\dot{M} - T_{\rm BZ}. \tag{12}$$

From the above two equations, it can be derived that

$$\frac{da_\bullet}{dt} = \frac{(\dot{M}L_{\rm in} - T_{\rm BZ})c}{G M_\bullet^2} - \frac{2a_\bullet(\dot{M}c^2 E_{\rm in} - P_{\rm BZ})}{M_\bullet c^2}, \tag{13}$$

where $\dot{M}$ is the accretion rate of the BH and $T_{\rm BZ}$ is the torque applied to the BH by the BZ process (L.-X. Li 2000; W.-H. Lei & Zhang 2011; W.-H. Lei et al. 2017):

$$T_{\rm BZ} = 3.4 \times 10^{45} a_\bullet^2 q^{-1} m_\bullet^3 B_{\bullet,15}^2 F(a_\bullet) \ {\rm g\,cm^2\,s^{-2}}. \tag{14}$$

Here, $E_{\rm in}$ and $L_{\rm in}$ are the specific energy and specific angular momentum at $R_{\rm isco}$, obtained from (I. D. Novikov & K. S. Thorne 1973)

$$E_{\rm in} = (4\sqrt{R_{\rm isco}} - 3a_\bullet)/(\sqrt{3}R_{\rm isco}), \tag{15}$$

$$L_{\rm in} = (GM_\bullet/c)[2(3\sqrt{R_{\rm isco}} - 2a_\bullet)]/(\sqrt{3R_{\rm isco}}), \tag{16}$$

with

$$R_{\rm isco}(M_\bullet, a_\bullet) = \frac{GM_\bullet}{c^2}\{3 + z_2 - [(3 - z_1)(3 + z_1 + 2z_2)]^{1/2}\},$$
$$z_1 = 1 + (1 - a_\bullet^2)^{1/3}[(1 + a_\bullet)^{1/3} + (1 - a_\bullet)^{1/3}],$$
$$z_2 = (3a_\bullet^2 + z_1^2)^{1/2}. \tag{17}$$

In the BZ process, the magnetic field plays a crucial role. The magnetic field lines thread the BH horizon and are connected to a remote astrophysical load. Thus, the rotational energy of the BH can be extracted through the BZ mechanism, launching a Poynting-flux-dominated jet. In addition, the magnetic field on a BH is maintained by an accretion disk, and magnetic flux can accumulate near the BH horizon. We can assume that the magnetic pressure of the BH is equal to the ram pressure of the accretion flow at the inner edge of the accretion disk, and estimate $B_\bullet$ as (R. Moderski et al. 1997)

$$\frac{B_\bullet^2}{8\pi} \approx \frac{\dot{M}c}{4\pi r_\bullet^2}, \tag{18}$$

where $r_\bullet = (1 + \sqrt{1 - a_\bullet^2})GM_\bullet/c^2$ is the radius of the BH horizon. From this, we can obtain

$$B_\bullet \approx 7.4 \times 10^{16} \dot{m}^{1/2} m_\bullet^{-1} (1 + \sqrt{1 - a_\bullet^2})^{-1} \ {\rm G}. \tag{19}$$

Based on the above assumption, the BZ jet power can be rewritten as a function of the accretion rate and spin for the BH:

$$L_{\rm BZ} = 9.3 \times 10^{53} \frac{a_\bullet^2 \dot{m} F(a_\bullet)}{(1 + \sqrt{1 - a_\bullet^2})^2} \ {\rm erg\ s^{-1}}, \tag{20}$$

where $\dot{m} = \dot{M}/(M_\odot\ {\rm s}^{-1})$.

3.3. Energy External Dissipation Mechanism

Suppose that a fraction ξ of BZ energy undergoes internal dissipation, and the remaining energy is injected into the blast wave of the GRB afterglow with relatively low velocity at time t_0, then if the injected energy is equal to or even greater than the kinetic energy of the blast wave, it will have an impact on the dynamic evolution of the blast wave. In the observer rest frame, the total kinetic energy of the blast wave is expressed as

$$E_k = (\Gamma - 1)(M_{\rm ej} + M_{\rm sw})c^2 + (1 - \varepsilon)\Gamma U + (1 - \xi)L_{\rm BZ} = E_0 + (1 - \xi)L_{\rm BZ}, \tag{21}$$

where Γ is the bulk Lorentz factor of the blast wave, $M_{\rm e}$ is the initial mass of the material ejected by the central engine, $M_{\rm sw}$ is the mass swept up by the blast wave, ε is the radiation efficiency, and U represents the internal energy of the blast wave. In addition, we introduce a parameter $\eta \equiv E_{\rm inj}/E_0$ to represent the ratio of the injected energy to the initial energy for the blast wave.

By differentiating Equation (21), we can obtain

$$\frac{d\Gamma}{dM_{\rm sw}} = -\frac{1}{M_{\rm ej} + 2\Gamma M_{\rm sw}}\left[\Gamma^2 - 1 - \frac{(1-\xi)L_{\rm BZ}}{c^2}\frac{dt}{dM_{\rm sw}}\right]. \tag{22}$$

To obtain the time evolution of Γ, the following three equations are required (Y. F. Huang et al. 2000):

$$\frac{dR}{dt} = \sqrt{\frac{\Gamma^2-1}{\Gamma}}c\Gamma(\Gamma + \sqrt{\Gamma^2-1}),$$
$$\frac{dM_{\rm sw}}{dR} = 2\pi R^2(1-\cos\theta)nm_p,$$
$$\frac{d\theta}{dt} = \frac{c_s(\Gamma + \sqrt{\Gamma^2-1})}{R}, \tag{23}$$

where R is the radius of the blast wave, θ is the opening angle of the jet, m_p is the mass of the proton, n is the particle number density of the unshocked environment, and c_s is the speed of sound, with

$$c_s^2 = \hat{\gamma}(\hat{\gamma}-1)(\Gamma-1)\frac{1}{1+\hat{\gamma}(\Gamma-1)}c^2. \tag{24}$$

Here, $\hat{\gamma} = (4\Gamma+1)/(3\Gamma)$ is the adiabatic index. By using the Runge–Kutta method, we can solve the group of differential equations composed of Equations (22) and (23).

Because the velocity of the blast wave is much greater than the speed of sound in the local frame, a strong forward shock will be formed. Electrons will be accelerated by the shock and will produce the bright broadband afterglow emission through synchrotron radiation. In the comoving frame of the ejecta, the total synchrotron radiation power of a single electron can be described by (G. B. Rybicki & A. P. Lightman 1979)

$$P(\gamma_e) = \frac{4}{3}\sigma_{\rm T}c\Gamma^2\gamma_e^2\frac{B'^2}{8\pi}, \tag{25}$$

where $\sigma_{\rm T}$ is the Thomson cross-section, γ_e is the electron Lorentz factor, and B' is the magnetic field strength in the comoving frame of the ejecta. Assuming that the density of magnetic field energy is a fixed proportion of the internal energy, i.e., the magnetic energy equipartition factor ϵ_B (R. Sari et al. 1998), then

$$B' = \sqrt{8\pi\epsilon_B(4\Gamma+3)(\Gamma-1)nm_pc^2} \approx \sqrt{32\pi\epsilon_B\Gamma^2 nm_pc^2}. \tag{26}$$

In the observer's rest frame, the observed characteristic frequency of radiation is (R. Sari et al. 1998)

$$\nu(\gamma_e) = \Gamma\gamma_e^2\frac{q_eB'}{8\pi}, \tag{27}$$

where q_e is the charge of the electron. Due to the monochromaticity of single-electron synchrotron radiation, the peak of its energy spectrum can be estimated as

$$P_{\nu,\rm max} \approx \frac{P(\gamma_e)}{\nu(\gamma_e)} = \frac{m_ec^2\sigma_T}{3q_e}B'\Gamma. \tag{28}$$

Assuming that the electrons accelerated by the shock follow a power-law distribution with Lorentz factor γ_e:

$$N(\gamma_e)d\gamma_e = C\gamma_e^{-p}d\gamma_e,\ \gamma_e > \gamma_m, \tag{29}$$

where C is a constant independent of the electron Lorentz factor. We assume that the ratio of electron energy to internal energy is a constant, that is, the electron energy equipartition factor ϵ_e is a constant. The minimum Lorentz factor γ_m of shock-accelerated electrons can be obtained by combining particle number conservation and energy conservation (R. Sari et al. 1998):

$$\gamma_m = \epsilon_e\frac{(p-2)m_p}{(p-1)m_e}(\Gamma-1). \tag{30}$$

According to the Equation (25), the higher the electron energy, the greater the radiated energy. Assuming that $\gamma_e = \gamma_c$, the energy radiated by the electron is equal to its kinetic energy, i.e.,

$$\Gamma\gamma_cm_ec^2 = P(\gamma_c). \tag{31}$$

The physical meaning is that electrons with $\gamma_e > \gamma_c$ will lose most of their energy due to synchrotron radiation, while for electrons with $\gamma_e < \gamma_c$ the cooling caused by synchrotron radiation can be ignored. From the definition of γ_c, we can obtain (R. Sari et al. 1998)

$$\gamma_c = \frac{6\pi m_ec}{\sigma_T\Gamma B'^2t} = \frac{3m_e}{16\epsilon_B\sigma_Tm_pct\Gamma^3n}. \tag{32}$$

We define

$$\nu_m \equiv \Gamma\frac{3q_eB'}{4\pi m_ec}\gamma_m^2,\quad \nu_c \equiv \Gamma\frac{3q_eB'}{4\pi m_ec}\gamma_c^2. \tag{33}$$

Based on the relationship between ν_m and ν_c, we can classify the cooling regime into two cases: the fast cooling regime ($\nu_c < \nu_m$) and the slow cooling regime ($\nu_c > \nu_m$). In the fast cooling regime, the observed flux is (R. Sari et al. 1998)

$$F_\nu = \begin{cases} (\nu/\nu_c)^{1/3}F_{\nu,\rm max}, & \nu < \nu_c, \\ (\nu/\nu_c)^{-1/2}F_{\nu,\rm max}, & \nu_c < \nu < \nu_m, \\ (\nu_m/\nu_c)^{-1/2}(\nu/\nu_m)^{-p/2}F_{\nu,\rm max}, & \nu_m < \nu. \end{cases} \tag{34}$$

In addition, the observed flux in the slow cooling regime is (R. Sari et al. 1998)

$$F_\nu = \begin{cases} (\nu/\nu_m)^{1/3}F_{\nu,\rm max}, & \nu < \nu_m, \\ (\nu/\nu_m)^{-(p-1)/2}F_{\nu,\rm max}, & \nu_m < \nu < \nu_c. \\ (\nu_c/\nu_m)^{-(p-1)/2}(\nu/\nu_c)^{-p/2}F_{\nu,\rm max}, & \nu_c < \nu, \end{cases} \tag{35}$$

In the above equations, $F_{\nu,\rm max}$ is the peak flux, which can be calculated from (R. Sari et al. 1998)

$$F_{\nu,\rm max} = \frac{N_{e,\rm tot}P_{\nu,\rm max}}{4\pi D_L^2}, \tag{36}$$

where D_L is the luminosity distance and $N_{e,\rm tot}$ is the total number of electrons swept up in the postshock medium.

Based on the above-mentioned fallback accretion model, BZ mechanism and energy external dissipation mechanism, we can calculate the light curve in any frequency range. In this paper, we focus on the light curve of the Swift/XRT energy band (0.3–10 keV).

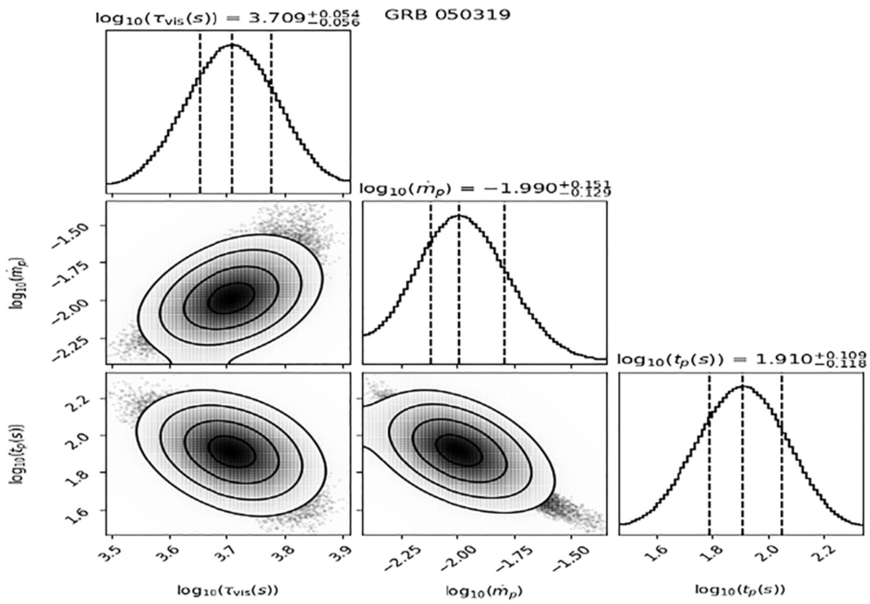

Figure 2. The posterior probability distribution of the free parameters of the sample obtained based on the MCMC fitting method. (The complete figure set (103 images) is available in the online article.)

4. Application of the Model to Selected GRBs

In the previous section, the physical model of fallback accretion energy external dissipation was introduced in detail. In this section, we apply this model to fit the shallow decay segment and the follow-up segment in our sample. In order to obtain the best fitting parameters in this complex model, we adopted the Markov Chain Monte Carlo (MCMC) method and the software is emcee (D. Foreman-Mackey et al. 2013). In emcee, we set the length of the Markov chain to 20,000. In order to obtain accurate fitting parameter values, we discarded the data of the first 5000 Markov chains. Furthermore, because there are few data for the shallow decay segment and follow-up segment in some GRBs and to reduce parameter degeneracy, we only selected the viscosity time of the accretion disk $\tau_{\rm vis}$, the peak of the dimensionless fallback rate $\dot{m}_p(\dot{m}_p = \dot{M}_p/(M_\odot\ {\rm s}^{-1}))$, and the peak time of the fallback rate t_p as the free parameters in the fitting. The boundaries of these three free parameters were set to $\log_{10}(\tau_{\rm vis}) \equiv [t_0, t_2]$, $\log_{10}(\dot{m}_p)) \equiv [-8, 0]$, and $\log_{10}(t_p) \equiv [t_0, t_2]$, respectively. Here, t_0 is the initial time when BZ energy is injected into the blast wave of the GRB afterglow, and we set $t_0 = 0.1 t_1$, where t_1 is the beginning time of the shallow decay segment, and t_2 is the end time of the follow-up segment. Other model parameters were set as follows: (1) fallback accretion mechanism: the spin of the BH increases with the accretion mechanism and decreases with the BZ mechanism, so it will reach an equilibrium value of ~0.87 (W.-H. Lei et al. 2017) and we set a_0 at this equilibrium value in our fitting; in addition, the peak sharpness of the fallback rate was set as $s = 3$; (2) BZ mechanism: it has been found that the initial mass of a BH hardly affects the BZ power, and here we set $M_{\bullet,0} = 3\ M_\odot$; (3) energy external dissipation mechanism: it is assumed that the radiation within the blast wave is adiabatic, $\epsilon = 0$, and all BZ energy is injected into the blast wave, $\xi = 0$; in addition, we set $E_0 = 10^{52}$ erg, $\Gamma_0 = 100$, $\theta_0 = 0.1$, $\epsilon_B = 10^{-4}$, $\epsilon_e = 0.1$, and $p = 2.5$.

The posterior probability distribution of the free parameters of the sample obtained based on the MCMC fitting method is shown in Figure 2. We adopt the median values of the posterior probability distribution of the free parameters and the 1σ confidence interval as fitting values and errors, and list them in Table 2. The fitting results for the shallow decay segments and the follow-up segments in our sample are shown in Figure 3. In addition, we also calculated several other quantities, including the ratio of the injected energy to the initial energy of the blast wave η, the magnetic field strength $B_{p,15}$ at the time t_p, the total accretion mass $M_{\rm acc}$, and the fallback radius at the time t_p. These values are also listed in Table 2.

The distributions of $\tau_{\rm vis}$, $\dot{m}_p$, t_p, η, $B_{p,15}$, $M_{\rm acc}$, and r_p for all GRBs in our sample are shown in Figure 4. We find that $\tau_{\rm vis}$, $\dot{m}_p$, t_p, η, $B_{p,15}$, $M_{\rm acc}$, and r_p follow log-normal distribution in the ranges 69.18–2.08×10^5 s, 2.75×10^{-7}–0.29, 6.31–1.95×10^4 s, 0.51–7.41×10^2, 0.01–1.44, 4.79×10^{-3}–1.20 $M_\odot$, and 1.04×10^9–2.45×10^{11} cm, respectively, with $\log_{10}(\tau_{\rm vis}({\rm s})) = 3.79 \pm 0.76$, $\log_{10}(\dot{m}_p) = -2.17 \pm 0.77$, $\log_{10}(t_p({\rm s})) = 1.83 \pm 0.66$, $\log_{10}(\eta) = 1.43 \pm 0.57$, $\log_{10}(B_{p,15}) = -0.71 \pm 0.40$, $\log_{10}(M_{\rm acc}(M_\odot)) = -0.83 \pm 0.42$, $\log_{10}(r_p({\rm cm})) = 9.71 \pm 0.44$.

Based on the fitting results, we can draw the following conclusions: (1) the fallback accretion energy external dissipation model can interpret the shallow decay segment and the follow-up segment in our sample within a reasonable parameter space; (2) during the fallback of progenitor envelope material, the progenitor stars of most GRBs have the highest fallback rate at a radius ~10^{10} cm, which is consistent with the typical radius of a Wolf–Rayet star; (3) the production of shallow decay segments for most GRBs in our sample requires the injection of BZ energy that is 10–100 times the kinetic energy of the initial GRB blast wave into the blast wave; however, for a few GRBs, the shallow decay segment requires an injected energy that is comparable to the kinetic energy of the blast wave, which means that even if less energy is injected into the GRB blast wave, it is still possible to produce a shallow decay segment; (4) the peak time of the fallback rate of the progenitor envelope material is close to the time when BZ energy is

Table 2
MCMC Fitting Results

GRB Name	$\log_{10}(\tau_{\rm vis})$ (s)	$\log_{10}(\dot{m}_p)$	$\log_{10}(t_p)$ (s)	$\log_{10}(\eta)$	$\log_{10}(B_{p,15})$ (G)	$\log_{10}(M_{\rm acc})$ ($M_\odot$)	$\log_{10}(r_p)$ (cm)	χ^2(dof)
050319	$3.709^{+0.054}_{-0.056}$	$-1.990^{+0.151}_{-0.129}$	$1.910^{+0.109}_{-0.118}$	1.49 ± 0.23	−0.45 ± 0.14	−0.47 ± 0.24	9.68 ± 0.05	128.96(90)
050401	$3.103^{+0.065}_{-0.059}$	$-0.845^{+0.513}_{-0.375}$	$1.263^{+0.155}_{-0.105}$	2.11 ± 0.11	−0.11 ± 0.05	-0.26 ± 0.09	9.23 ± 0.07	450.01(318)
050416A	$4.229^{+0.034}_{-0.034}$	$-0.692^{+0.040}_{-0.073}$	$1.011^{+0.001}_{-0.001}$	2.24 ± 0.01	−1.02 ± 0.02	−1.5 ± 0.02	9.35 ± 0.01	145.6(92)
050714B	$5.313^{+0.092}_{-0.089}$	$-1.788^{+0.584}_{-0.448}$	$2.756^{+0.005}_{-0.003}$	2.86 ± 0.27	−1.28 ± 0.12	−0.83 ± 0.22	10.28 ± 0.01	19.73(12)
050802	$3.318^{+0.054}_{-0.073}$	$-2.608^{+0.332}_{-0.456}$	$2.085^{+0.233}_{-0.093}$	1.36 ± 0.31	−0.57 ± 0.16	−0.84 ± 0.22	9.97 ± 0.06	210.32(142)
050822	$4.746^{+0.062}_{-0.062}$	$-2.744^{+0.528}_{-0.374}$	$2.321^{+0.142}_{-0.092}$	1.46 ± 0.24	−1.09 ± 0.18	−0.49 ± 0.25	10.11 ± 0.04	152.01(91)
050824	$5.105^{+0.036}_{-0.035}$	$-3.755^{+0.452}_{-0.358}$	$2.982^{+0.131}_{-0.082}$	1.19 ± 0.21	−1.49 ± 0.16	−0.82 ± 0.32	10.65 ± 0.04	70.38(37)
050826	$3.951^{+0.041}_{-0.055}$	$-6.582^{+0.294}_{-0.241}$	$4.041^{+0.142}_{-0.124}$	−0.27 ± 0.21	−1.98 ± 0.19	−2.31 ± 0.32	11.40 ± 0.27	1.24(6)
051221A	$4.761^{+0.040}_{-0.038}$	$-2.337^{+0.752}_{-0.468}$	$1.880^{+0.009}_{-0.007}$	1.63 ± 0.31	−1.56 ± 0.19	−1.53 ± 0.40	10.05 ± 0.03	90.32(53)
060108	$4.281^{+0.045}_{-0.050}$	$-0.996^{+0.386}_{-0.346}$	$1.668^{+0.005}_{-0.003}$	2.53 ± 0.44	−0.81 ± 0.15	−1.12 ± 0.26	9.61 ± 0.01	47.24(25)
060115	$4.150^{+0.055}_{-0.057}$	$-1.188^{+0.317}_{-0.386}$	$1.918^{+0.005}_{-0.003}$	2.35 ± 0.35	−0.72 ± 0.21	−0.88 ± 0.34	9.69 ± 0.01	38.91(23)
060306	$3.898^{+0.032}_{-0.033}$	$-1.482^{+0.109}_{-0.170}$	$1.594^{+0.001}_{-0.001}$	2.00 ± 0.59	−0.79 ± 0.14	−0.95 ± 0.29	9.62 ± 0.01	95.89(76)
060502A	$4.437^{+0.031}_{-0.032}$	$-1.266^{+0.257}_{-0.338}$	$1.415^{+0.009}_{-0.005}$	2.14 ± 0.36	−0.92 ± 0.28	−0.60 ± 0.32	9.54 ± 0.02	62.12(54)
060604	$4.469^{+0.035}_{-0.069}$	$-2.503^{+0.502}_{-0.702}$	$2.624^{+0.008}_{-0.002}$	1.82 ± 0.53	−0.98 ± 0.14	−0.76 ± 0.26	10.24 ± 0.01	97.61(65)
060605	$3.343^{+0.073}_{-0.059}$	$-0.925^{+0.509}_{-0.634}$	$1.289^{+0.117}_{-0.028}$	1.87 ± 0.43	−0.35 ± 0.16	−0.75 ± 0.27	9.24 ± 0.03	89.22(72)
060614	$4.476^{+0.048}_{-0.048}$	$-5.669^{+0.155}_{-0.127}$	$3.323^{+0.106}_{-0.119}$	−0.14 ± 0.05	−1.89 ± 0.07	−1.92 ± 0.11	11.00 ± 0.05	192.23(150)
060707	$4.309^{+0.035}_{-0.053}$	$-2.197^{+0.043}_{-0.138}$	$2.014^{+0.003}_{-0.001}$	1.51 ± 0.17	−0.66 ± 0.11	−0.34 ± 0.08	9.73 ± 0.03	60.21(33)
060714	$3.494^{+0.042}_{-0.115}$	$-1.881^{+0.324}_{-0.932}$	$1.603^{+0.045}_{-0.005}$	1.45 ± 0.32	−0.51 ± 0.26	−0.78 ± 0.24	9.54 ± 0.02	82.46(47)
060719	$3.853^{+0.041}_{-0.055}$	$-1.345^{+0.500}_{-0.535}$	$1.796^{+0.007}_{-0.003}$	2.21 ± 0.35	−0.85 ± 0.21	−1.18 ± 0.21	9.72 ± 0.02	59.13(50)
060729	$4.881^{+0.027}_{-0.027}$	$-2.552^{+0.348}_{-0.337}$	$2.055^{+0.168}_{-0.106}$	2.22 ± 0.37	−0.83 ± 0.22	−1.16 ± 0.26	10.06 ± 0.05	1003.24(706)
060805A	$3.267^{+0.071}_{-0.074}$	$-2.439^{+0.088}_{-0.138}$	$1.301^{+0.002}_{-0.001}$	0.53 ± 0.16	−0.85 ± 0.08	−1.67 ± 0.19	9.33 ± 0.01	16.03(8)
060814	$4.020^{+0.066}_{-0.063}$	$-2.186^{+0.900}_{-0.577}$	$2.236^{+0.172}_{-0.068}$	1.67 ± 0.24	−0.75 ± 0.16	−0.59 ± 0.21	10.05 ± 0.04	270.31(163)
060906	$3.768^{+0.050}_{-0.047}$	$-2.293^{+0.495}_{-0.339}$	$1.967^{+0.139}_{-0.102}$	1.26 ± 0.24	−0.65 ± 0.13	−0.91 ± 0.27	9.65 ± 0.04	64.36(32)
060908	$1.839^{+0.204}_{-0.205}$	$-2.307^{+0.232}_{-0.233}$	$1.094^{+0.220}_{-0.218}$	0.59 ± 0.25	−0.13 ± 0.08	−1.39 ± 0.18	9.25 ± 0.04	65.83(33)
061121	$3.527^{+0.060}_{-0.092}$	$-2.016^{+0.389}_{-0.664}$	$1.593^{+0.051}_{-0.010}$	1.49 ± 0.29	−0.51 ± 0.15	−0.55 ± 0.19	9.64 ± 0.02	356.45(269)
070103	$3.092^{+0.060}_{-0.054}$	$-1.836^{+0.501}_{-0.339}$	$1.284^{+0.060}_{-0.038}$	1.13 ± 0.26	−0.54 ± 0.14	−1.31 ± 0.19	9.32 ± 0.02	34.72(24)
070129	$4.401^{+0.074}_{-0.133}$	$-2.793^{+0.597}_{-1.494}$	$2.412^{+0.114}_{-0.007}$	1.41 ± 0.25	−0.88 ± 0.16	−0.57 ± 0.22	10.06 ± 0.04	158.63(80)
070306	$4.276^{+0.041}_{-0.035}$	$-1.873^{+0.407}_{-0.404}$	$1.852^{+0.135}_{-0.065}$	1.84 ± 0.21	−0.79 ± 0.18	−0.43 ± 0.19	9.79 ± 0.04	198.51(141)
070508	$2.372^{+0.057}_{-0.050}$	$-2.276^{+0.515}_{-0.371}$	$1.061^{+0.152}_{-0.101}$	0.89 ± 0.24	−0.28 ± 0.16	−1.11 ± 0.25	9.36 ± 0.05	623.05(484)
070521	$3.149^{+0.053}_{-0.044}$	$-1.646^{+0.426}_{-0.385}$	$0.595^{+0.102}_{-0.051}$	0.53 ± 0.33	−0.78 ± 0.09	−1.34 ± 0.19	9.30 ± 0.08	164.23(74)
070529	$2.876^{+0.047}_{-0.061}$	$-2.237^{+0.458}_{-0.382}$	$1.506^{+0.184}_{-0.117}$	0.98 ± 0.29	−0.42 ± 0.11	−1.12 ± 0.24	9.46 ± 0.06	36.21(30)
070810A	$2.958^{+0.119}_{-0.060}$	$-1.771^{+0.720}_{-0.455}$	$1.182^{+0.119}_{-0.059}$	1.06 ± 0.34	−0.51 ± 0.16	−1.26 ± 0.22	9.28 ± 0.01	46.32(31)
080310	$3.877^{+0.057}_{-0.060}$	$-2.112^{+0.570}_{-0.458}$	$2.134^{+0.203}_{-0.111}$	−0.22 ± 0.03	−0.29 ± 0.21	0.01 ± 0.03	9.88 ± 0.20	90.58(68)
080413B	$2.868^{+0.077}_{-0.129}$	$-2.359^{+0.358}_{-0.366}$	$1.386^{+0.292}_{-0.216}$	0.93 ± 0.28	−0.45 ± 0.13	−1.04 ± 0.28	9.54 ± 0.03	470.25(233)
080430	$4.527^{+0.040}_{-0.052}$	$-2.943^{+0.402}_{-0.376}$	$1.956^{+0.168}_{-0.098}$	1.00 ± 0.31	−1.21 ± 0.17	−0.86 ± 0.26	9.98 ± 0.05	160.14(141)
080516	$3.546^{+0.044}_{-0.065}$	$-2.076^{+0.071}_{-0.207}$	$1.381^{+0.004}_{-0.001}$	0.94 ± 0.18	−0.62 ± 0.32	−1.01 ± 0.23	9.31 ± 0.05	49.65(27)
080707	$4.190^{+0.062}_{-0.060}$	$-1.352^{+0.504}_{-0.442}$	$1.410^{+0.009}_{-0.005}$	1.96 ± 0.31	−1.07 ± 0.21	−1.27 ± 0.43	9.53 ± 0.01	24.17(22)
080905B	$3.234^{+0.003}_{-0.004}$	$-1.825^{+0.081}_{-0.125}$	$1.509^{+0.047}_{-0.026}$	1.46 ± 0.32	−0.32 ± 0.11	−0.63 ± 0.23	9.48 ± 0.06	120.53(78)
081029	$3.739^{+0.058}_{-0.059}$	$-2.836^{+0.456}_{-0.272}$	$2.673^{+0.153}_{-0.158}$	1.41 ± 0.21	−0.54 ± 0.28	−0.61 ± 0.24	10.15 ± 0.06	160.31(80)
081221	$2.692^{+0.054}_{-0.056}$	$-1.417^{+0.358}_{-0.308}$	$1.519^{+0.131}_{-0.082}$	1.81 ± 0.36	−0.06 ± 0.16	−0.56 ± 0.29	9.49 ± 0.10	332.67(256)
090113	$2.718^{+0.082}_{-0.065}$	$-1.660^{+0.568}_{-0.432}$	$1.055^{+0.075}_{-0.035}$	0.73 ± 0.25	−0.42 ± 0.17	−1.23 ± 0.21	9.43 ± 0.02	36.27(22)
090205	$3.478^{+0.024}_{-0.025}$	$-2.173^{+0.024}_{-0.050}$	$1.782^{+0.001}_{-0.000}$	1.21 ± 0.13	−0.52 ± 0.05	−0.95 ± 0.11	9.51 ± 0.01	52.16(30)
090313	$3.611^{+0.347}_{-0.113}$	$-4.328^{+0.159}_{-0.029}$	$4.289^{+0.089}_{-0.229}$	1.61 ± 0.35	−0.76 ± 0.05	−0.43 ± 0.11	11.26 ± 0.07	30.14(27)
090404	$4.329^{+0.044}_{-0.105}$	$-1.995^{+0.340}_{-0.762}$	$1.785^{+0.059}_{-0.059}$	1.55 ± 0.27	−0.70 ± 0.15	−0.39 ± 0.16	9.61 ± 0.08	210.16(109)
090407	$4.704^{+0.044}_{-0.043}$	$-1.384^{+0.442}_{-0.306}$	$2.080^{+0.005}_{-0.005}$	2.45 ± 0.22	−1.01 ± 0.21	−0.73 ± 0.21	9.97 ± 0.01	156.32(107)
090418A	$3.089^{+0.044}_{-0.053}$	$-2.052^{+0.381}_{-0.376}$	$1.361^{+0.255}_{-0.171}$	1.14 ± 0.23	−0.44 ± 0.21	−0.85 ± 0.22	9.45 ± 0.10	126.51(103)
090424	$3.281^{+0.036}_{-0.038}$	$-0.877^{+0.100}_{-0.172}$	$1.514^{+0.001}_{-0.001}$	2.59 ± 0.26	−0.52 ± 0.18	−0.92 ± 0.29	9.66 ± 0.01	140.22(101)
090529	$4.863^{+0.155}_{-0.131}$	$-3.237^{+1.242}_{-0.715}$	$2.711^{+0.461}_{-0.232}$	1.19 ± 0.51	−1.23 ± 0.21	−0.78 ± 0.27	10.25 ± 0.16	3.29(5)
090530	$4.477^{+0.037}_{-0.038}$	$-1.864^{+0.054}_{-0.104}$	$1.317^{+0.001}_{-0.001}$	1.34 ± 0.30	−1.18 ± 0.17	−0.98 ± 0.23	9.46 ± 0.01	56.25(40)
091018	$2.544^{+0.067}_{-0.065}$	$-2.499^{+0.460}_{-0.379}$	$1.154^{+0.112}_{-0.062}$	0.56 ± 0.21	−0.47 ± 0.15	−1.33 ± 0.18	9.36 ± 0.03	241.86(139)
091029	$4.103^{+0.083}_{-0.085}$	$-2.082^{+0.760}_{-0.489}$	$1.940^{+0.305}_{-0.199}$	1.58 ± 0.28	−0.74 ± 0.11	−0.64 ± 0.22	9.75 ± 0.04	194.07(122)
100302A	$4.532^{+0.041}_{-0.041}$	$-2.245^{+0.396}_{-0.357}$	$2.319^{+0.176}_{-0.114}$	1.48 ± 0.14	−0.83 ± 0.11	−0.62 ± 0.13	9.86 ± 0.02	25.49(20)
100418A	$5.049^{+0.055}_{-0.059}$	$-4.866^{+0.148}_{-0.120}$	$3.412^{+0.116}_{-0.141}$	0.62 ± 0.12	−1.65 ± 0.11	−1.08 ± 0.13	10.94 ± 0.06	30.49(22)
100425A	$4.310^{+0.061}_{-0.064}$	$-3.096^{+0.456}_{-0.488}$	$1.934^{+0.355}_{-0.216}$	0.66 ± 0.21	−1.18 ± 0.12	−1.21 ± 0.21	9.82 ± 0.14	16.90(15)
100901A	$4.538^{+0.039}_{-0.037}$	$-3.041^{+0.392}_{-0.249}$	$2.831^{+0.124}_{-0.126}$	1.71 ± 0.18	−0.92 ± 0.09	−0.36 ± 0.11	10.49 ± 0.05	550.76(267)
110106B	$3.855^{+0.036}_{-0.039}$	$-1.472^{+0.374}_{-0.510}$	$1.503^{+0.004}_{-0.001}$	2.07 ± 0.13	−1.03 ± 0.07	−1.48 ± 0.14	9.69 ± 0.01	68.28(50)
110213A	$3.281^{+0.147}_{-0.100}$	$-1.786^{+0.660}_{-0.175}$	$1.275^{+0.179}_{-0.556}$	2.01 ± 0.35	−0.37 ± 0.10	−0.58 ± 0.18	9.40 ± 0.08	401.9(257)

Table 2
(Continued)

GRB Name	$\log_{10}(\tau_{vis})$ (s)	$\log_{10}(\dot{m}_p)$	$\log_{10}(t_p)$ (s)	$\log_{10}(\eta)$	$\log_{10}(B_{p,15})$ (G)	$\log_{10}(M_{acc})$ ($M_\odot$)	$\log_{10}(r_p)$ (cm)	χ^2(dof)
110808A	$4.919^{+0.071}_{-0.068}$	$-2.673^{+0.661}_{-0.485}$	$1.884^{+0.291}_{-0.199}$	1.12 ± 0.24	−1.42 ± 0.31	−1.02 ± 0.30	9.83 ± 0.09	6.16(9)
111008A	$3.485^{+0.035}_{-0.037}$	$-1.689^{+0.343}_{-0.286}$	$1.798^{+0.105}_{-0.073}$	1.58 ± 0.22	−0.18 ± 0.07	−0.36 ± 0.11	9.50 ± 0.07	213.22(135)
111228A	$4.035^{+0.165}_{-0.166}$	$-2.811^{+0.813}_{-0.589}$	$1.913^{+0.385}_{-0.257}$	1.11 ± 0.33	−0.97 ± 0.21	−0.86 ± 0.22	9.94 ± 0.14	193.17(150)
120326A	$4.616^{+0.052}_{-0.054}$	$-3.265^{+0.129}_{-0.110}$	$3.275^{+0.047}_{-0.050}$	1.81 ± 0.28	−0.87 ± 0.06	−0.18 ± 0.12	10.71 ± 0.02	375.74(191)
120404A	$3.198^{+0.050}_{-0.050}$	$-1.834^{+0.571}_{-0.418}$	$1.700^{+0.125}_{-0.067}$	1.47 ± 0.48	−0.37 ± 0.05	−0.89 ± 0.11	9.56 ± 0.08	49.76(36)
120521C	$3.946^{+0.083}_{-0.082}$	$-2.197^{+0.695}_{-0.834}$	$2.014^{+0.118}_{-0.022}$	1.22 ± 0.33	−0.58 ± 0.18	−0.82 ± 0.27	9.61 ± 0.05	6.13(7)
120811C	$3.436^{+0.036}_{-0.110}$	$-1.992^{+0.279}_{-1.051}$	$1.633^{+0.062}_{-0.004}$	1.36 ± 0.25	−0.40 ± 0.10	−0.68 ± 0.20	9.54 ± 0.06	70.69(45)
120907A	$3.217^{+0.103}_{-0.117}$	$-2.407^{+0.823}_{-0.576}$	$1.045^{+0.376}_{-0.233}$	0.63 ± 0.31	−0.80 ± 0.25	−1.36 ± 0.35	9.32 ± 0.12	155.51(87)
120118B	$3.876^{+0.056}_{-0.066}$	$-1.776^{+0.477}_{-0.527}$	$1.704^{+0.194}_{-0.074}$	1.63 ± 0.50	−0.64 ± 0.09	−0.73 ± 0.19	9.56 ± 0.08	35.61(30)
121128A	$2.301^{+0.063}_{-0.064}$	$-2.051^{+0.128}_{-0.151}$	$1.374^{+0.125}_{-0.143}$	1.08 ± 0.26	−1.11 ± 0.13	−0.98 ± 0.21	9.39 ± 0.05	179.12(95)
131105A	$3.702^{+0.030}_{-0.030}$	$-2.515^{+0.395}_{-0.356}$	$1.828^{+0.176}_{-0.113}$	1.11 ± 0.29	−0.74 ± 0.17	−0.94 ± 0.26	9.77 ± 0.13	70.23(49)
140206A	$3.332^{+0.018}_{-0.020}$	$-1.856^{+0.072}_{-0.138}$	$2.059^{+0.031}_{-0.013}$	1.88 ± 0.52	−0.09 ± 0.10	−0.01 ± 0.02	9.81 ± 0.08	702.11(451)
140430A	$4.329^{+0.048}_{-0.052}$	$-1.645^{+0.518}_{-0.517}$	$1.691^{+0.011}_{-0.005}$	1.88 ± 0.23	−1.02 ± 0.16	−0.96 ± 0.26	9.68 ± 0.02	39.38(37)
140509A	$3.714^{+0.360}_{-0.372}$	$-3.061^{+0.578}_{-0.109}$	$2.697^{+0.253}_{-0.475}$	1.34 ± 0.68	−0.81 ± 0.11	−1.06 ± 0.23	10.26 ± 0.10	12.26(19)
140518A	$2.784^{+0.206}_{-0.209}$	$-3.305^{+0.277}_{-0.127}$	$2.728^{+0.179}_{-0.270}$	0.91 ± 0.32	−0.34 ± 0.12	−0.93 ± 0.17	10.11 ± 0.10	36.12(28)
140703A	$3.239^{+0.123}_{-0.119}$	$-1.656^{+0.210}_{-0.146}$	$1.637^{+0.133}_{-0.166}$	1.58 ± 0.25	−0.17 ± 0.09	−0.39 ± 0.15	9.51 ± 0.06	145.08(76)
141121A	$5.054^{+0.075}_{-0.118}$	$-4.285^{+0.408}_{-0.373}$	$3.927^{+0.292}_{-0.229}$	1.48 ± 0.24	−1.25 ± 0.08	−0.36 ± 0.22	11.21 ± 0.11	23.16(22)
150314A	$3.465^{+0.045}_{-0.045}$	$-3.333^{+0.382}_{-0.307}$	$2.982^{+0.068}_{-0.043}$	1.68 ± 0.64	−0.43 ± 0.06	−0.27 ± 0.14	10.47 ± 0.09	155.23(94)
150323A	$4.276^{+0.088}_{-0.087}$	$-1.828^{+0.637}_{-0.549}$	$1.654^{+0.005}_{-0.003}$	1.88 ± 0.33	−1.31 ± 0.15	−1.62 ± 0.23	9.81 ± 0.01	31.16(18)
150403A	$2.951^{+0.063}_{-0.064}$	$-0.518^{+0.151}_{-0.127}$	$1.034^{+0.125}_{-0.144}$	2.19 ± 0.38	0.16 ± 0.27	−0.07 ± 0.16	9.15 ± 0.08	2182.32(1721)
150910A	$2.722^{+0.029}_{-0.027}$	$-2.761^{+0.139}_{-0.127}$	$2.316^{+0.001}_{-0.001}$	1.43 ± 0.14	−0.26 ± 0.13	−0.59 ± 0.18	10.12 ± 0.01	640.71(336)
151027A	$3.467^{+0.032}_{-0.035}$	$-2.236^{+0.280}_{-0.300}$	$1.849^{+0.105}_{-0.059}$	1.58 ± 0.37	−0.58 ± 0.18	−0.62 ± 0.30	9.89 ± 0.04	651.48(445)
151112A	$4.063^{+0.036}_{-0.037}$	$-3.150^{+0.334}_{-0.250}$	$3.134^{+0.117}_{-0.105}$	1.33 ± 0.23	−0.67 ± 0.05	−0.51 ± 0.11	10.46 ± 0.01	32.18(29)
160121A	$3.723^{+0.062}_{-0.080}$	$-2.782^{+0.153}_{-0.396}$	$1.805^{+0.019}_{-0.005}$	0.84 ± 0.68	−0.87 ± 0.29	−1.12 ± 0.52	9.74 ± 0.09	24.54(21)
160227A	$4.152^{+0.053}_{-0.059}$	$-2.499^{+0.134}_{-0.118}$	$2.466^{+0.051}_{-0.053}$	1.75 ± 0.38	−0.62 ± 0.05	−0.23 ± 0.11	10.13 ± 0.01	202.87(102)
160327A	$3.313^{+0.054}_{-0.046}$	$-1.727^{+0.438}_{-0.356}$	$1.657^{+0.122}_{-0.073}$	1.43 ± 0.34	−0.36 ± 0.19	−0.86 ± 0.27	9.40 ± 0.05	55.19(26)
160804A	$4.764^{+0.060}_{-0.058}$	$-1.623^{+0.105}_{-0.182}$	$2.012^{+0.003}_{-0.001}$	2.40 ± 0.43	−1.27 ± 0.27	−1.00 ± 0.33	10.00 ± 0.01	70.93(43)
161108A	$5.177^{+0.107}_{-0.098}$	$-1.417^{+0.654}_{-1.197}$	$1.843^{+0.214}_{-0.019}$	1.13 ± 0.33	−1.31 ± 0.13	−0.80 ± 0.28	10.02 ± 0.02	30.32(24)
161129A	$3.128^{+0.040}_{-0.045}$	$-3.013^{+0.399}_{-0.338}$	$1.606^{+0.142}_{-0.091}$	0.63 ± 0.28	−0.89 ± 0.09	−1.54 ± 0.21	9.75 ± 0.05	98.86(53)
170113A	$3.341^{+0.051}_{-0.061}$	$-2.070^{+0.604}_{-0.438}$	$1.588^{+0.151}_{-0.079}$	1.32 ± 0.32	−0.43 ± 0.16	−0.67 ± 0.27	9.64 ± 0.13	220.21(149)
170202A	$3.492^{+0.034}_{-0.042}$	$-1.769^{+0.368}_{-0.318}$	$1.685^{+0.154}_{-0.109}$	1.42 ± 0.30	−0.36 ± 0.15	−0.59 ± 0.26	9.53 ± 0.03	52.37(39)
170705A	$3.675^{+0.069}_{-0.067}$	$-2.157^{+0.461}_{-0.381}$	$2.035^{+0.112}_{-0.062}$	1.66 ± 1.03	−0.44 ± 0.09	−0.33 ± 0.19	9.84 ± 0.08	438.37(215)
170903A	$4.436^{+0.050}_{-0.077}$	$-3.529^{+0.524}_{-0.609}$	$2.703^{+0.005}_{-0.002}$	1.18 ± 0.16	−1.20 ± 0.06	−0.92 ± 0.21	10.44 ± 0.01	73.54(51)
171222A	$5.197^{+0.105}_{-0.103}$	$-2.472^{+0.721}_{-1.016}$	$2.346^{+0.216}_{-0.029}$	1.43 ± 0.39	−1.13 ± 0.28	−0.49 ± 0.29	10.03 ± 0.13	11.38(10)
180115A	$3.296^{+0.041}_{-0.048}$	$-2.215^{+0.375}_{-0.348}$	$1.708^{+0.147}_{-0.088}$	1.14 ± 0.35	−0.57 ± 0.11	−0.96 ± 0.25	9.59 ± 0.04	39.03(49)
180329B	$3.530^{+0.055}_{-0.062}$	$-2.456^{+0.514}_{-0.388}$	$1.947^{+0.193}_{-0.131}$	1.25 ± 0.57	−0.62 ± 0.20	−0.78 ± 0.45	9.83 ± 0.07	58.33(49)
180404A	$3.846^{+0.052}_{-0.053}$	$-2.531^{+0.023}_{-0.053}$	$1.312^{+0.001}_{-0.000}$	0.69 ± 0.29	−1.10 ± 0.16	−1.38 ± 0.24	9.51 ± 0.10	0.98(3)
180620B	$4.537^{+0.051}_{-0.056}$	$-2.514^{+0.568}_{-0.463}$	$2.308^{+0.173}_{-0.086}$	1.71 ± 0.34	−0.94 ± 0.21	−0.39 ± 0.20	10.13 ± 0.12	154.81(81)
181010A	$3.008^{+0.057}_{-0.070}$	$-1.689^{+0.764}_{-0.488}$	$0.803^{+0.301}_{-0.198}$	0.99 ± 0.33	−0.45 ± 0.09	−0.97 ± 0.19	9.11 ± 0.10	290.92(116)
190106A	$3.650^{+0.046}_{-0.049}$	$-2.061^{+0.149}_{-0.126}$	$1.826^{+0.106}_{-0.115}$	1.53 ± 0.34	−0.47 ± 0.05	−0.40 ± 0.11	9.73 ± 0.04	131.31(91)
190114A	$3.419^{+0.042}_{-0.044}$	$-1.813^{+0.441}_{-0.400}$	$1.684^{+0.177}_{-0.100}$	1.62 ± 0.33	−0.38 ± 0.19	−0.65 ± 0.32	9.51 ± 0.03	90.17(70)
201221A	$3.421^{+0.022}_{-0.023}$	$-1.988^{+0.025}_{-0.041}$	$1.940^{+0.001}_{-0.000}$	1.35 ± 0.23	−0.31 ± 0.11	−0.64 ± 0.25	9.55 ± 0.04	20.26(15)
210104A	$2.919^{+0.072}_{-0.057}$	$-2.166^{+0.506}_{-0.467}$	$1.135^{+0.146}_{-0.065}$	1.06 ± 0.32	−0.67 ± 0.21	−1.28 ± 0.29	9.47 ± 0.04	919.63(620)
210210A	$3.110^{+0.026}_{-0.027}$	$-2.192^{+0.052}_{-0.104}$	$0.829^{+0.001}_{-0.001}$	0.54 ± 0.13	−0.82 ± 0.11	−1.41 ± 0.30	9.35 ± 0.01	108.9(77)
210610A	$3.121^{+0.060}_{-0.062}$	$-1.589^{+0.137}_{-0.121}$	$1.127^{+0.057}_{-0.061}$	1.12 ± 0.21	−0.32 ± 0.12	−0.83 ± 0.24	9.13 ± 0.03	41.24(34)
230325A	$4.406^{+0.196}_{-0.197}$	$-3.485^{+0.814}_{-0.599}$	$3.410^{+0.390}_{-0.284}$	1.71 ± 0.32	−1.02 ± 0.12	−0.62 ± 0.19	10.81 ± 0.11	24.27(16)

injected into the shock wave, which means that the fallback accretion is more active in the initial phase.

It is worth noting that a few GRBs in our sample, such as GRB 070103, exhibit shallow decay segments with negative decay slopes. In such cases, it is not easy to obtain a good fit using the external dissipation model of fallback accretion energy. For these sources, we believe that the internal dissipation component of fallback accretion energy should dominate the radiation during this phase.

5. Test of Fallback Rate

Based on the fitting results, it is known that the fallback rate of the progenitor envelope materials onto the accretion disk can reach a peak of 10^{-7}–0.1 $M_\odot$ s^{-1} at times ranging from 10–10^5 s. Next, we will test whether the progenitor of the GRB can provide enough envelope materials to satisfy the accretion of the BH.

Assuming that the progenitor star is symmetric about its rotation axis and mirror-symmetric across the equator, when a

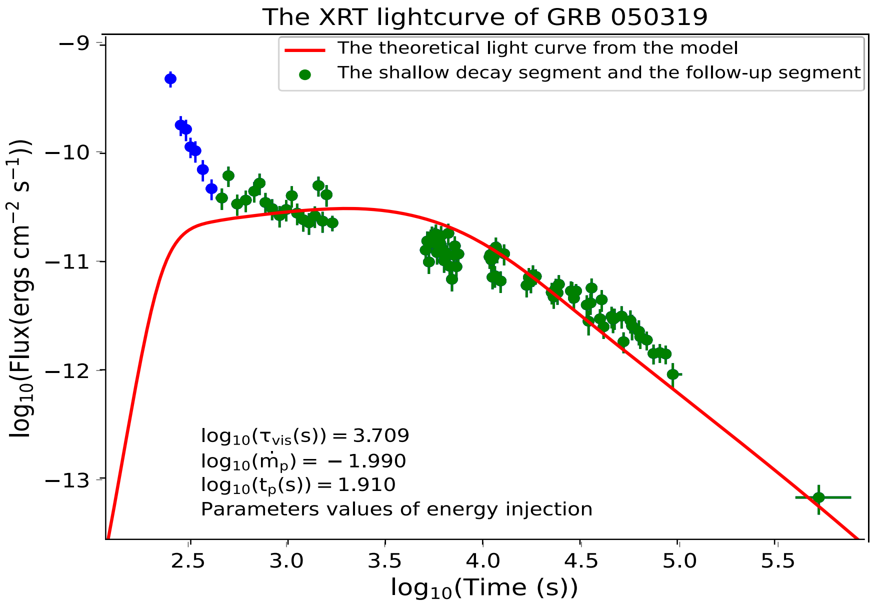

Figure 3. The fitting results of shallow decay segments and follow-up segments in our sample.
(The complete figure set (103 images) is available in the online article.)

particle (Particle 1) falls back from its initial position to the equatorial plane, it will collide with another particle (Particle 2) with a velocity of $-v_z$ in the equatorial plane. The positions of the two particles are mirror-symmetric across the equator; see Figure 1 in P. Kumar et al. (2008). The time it takes for a particle with an initial position (r, θ, ϕ) and an angular velocity Ω to fall back to the equatorial plane of the progenitor star at the end of its evolution is approximately (P. Kumar et al. 2008)

$$t_{\rm eq} \approx t_{\rm s}(r) + \frac{\pi}{2^{3/2}\Omega_{\rm k}}\left[1 + \frac{3}{4}\left(\frac{\Omega\sin\theta}{\Omega_{\rm k}}\right)^2\right], \tag{37}$$

where $\Omega_{\rm k}$ is the local Kepler angular velocity of the particle, and $t_s(r)$ is the sound propagation time from the center of the progenitor star to the initial position of the particle.

We assume that the difference between the polar and equatorial radii of an equal-collapse-time surface is δ_r. For a given $t_{\rm eq}$, the radial difference between particles starting from $\theta = 0$ and from $\theta = \pi/2$ is (P. Kumar et al. 2008)

$$\delta r = \frac{3\pi}{2^{7/2}}\frac{[\Omega(r)/\Omega_{\mathbf{k}}(r)]^2}{\Omega_{\mathbf{k}}(r)d(t_s + \pi 2^{-3/2}\Omega_{\mathbf{k}}^{-1})/dr}. \tag{38}$$

Additionally, we define

$$H_t^{-1} \equiv \left|\frac{d}{dr}\ln[t_s + \pi 2^{-3/2}\Omega_k^{-1}]\right|. \tag{39}$$

Combining Equations (38) and (39), one obtains (P. Kumar et al. 2008)

$$\delta r \sim \frac{H_t}{2}\left[\frac{\Omega(r)}{\Omega_{\mathbf{k}}(r)}\right]^2. \tag{40}$$

In the above equation, we assume $t_s \sim \Omega_k^{-1}$, which is valid outside a relatively small core region. Since $\delta_r \ll r$, we can approximate the equal-collapse-time surface as a sphere. The fallback rate of materials on the equatorial plane of the progenitor star should be equal to the mass loss rate of the progenitor star per unit time (P. Kumar et al. 2008):

$$\dot{M}_{\rm eq,fb}(t_{\rm eq}) \approx \frac{dM(r)}{dr}\frac{dr}{dt_{\rm eq}} \approx \frac{4\pi r^2\rho(r)}{t_{\rm eq}|d\ln\Omega_{\rm k}/{\rm d}r|}. \tag{41}$$

After fallback to the equatorial plane of a star, the velocity of the materials can be decomposed into a ϕ component around the equatorial plane and an r component toward the center. The velocity components in the two directions satisfy $|v_r| > v_\phi$, where the sign of v_r is negative and independent of the initial position of the particle. This will cause the initial disk formed during the core collapse process to shrink rapidly toward the center, terminating when it reaches a radius defined as the fallback radius $r_{\rm fb}$:

$$r_{\rm fb} \approx r\left(\frac{\Omega}{\Omega_k}\right)^2. \tag{42}$$

At the fallback radius, the specific angular momentum of the inflowing materials is equal to that of the local circular orbit. If its fallback radius $r_{\rm fb}$ is smaller than the radius $R_{\rm isco}$ of the BH, a BH will be directly formed. Otherwise, an accretion disk will be formed around the BH. It is worth noting that the timescale for shrinkage of the initial disk is much shorter than $t_{\rm eq}$. Therefore, we can equate the fallback rate of materials onto the accretion disk with the fallback rate of materials onto the equatorial plane, i.e., $\dot{M}_{\rm eq,fb} = \dot{M}_{\rm fb}$. Assuming the formation time of the initial BH is $t_{\rm BH}$, and given the density and spin profiles of the progenitor, we can obtain the fallback rate of the star's material onto the accretion disk $\dot{M}_{\rm fb}(t)$, where $t = t_{\rm eq} - t_{\rm BH}$.

T. Liu et al. (2018) provided the density profiles of progenitors with different metallicities and masses. The spin profile was given by P. Kumar et al. (2008). Figure 5 shows the evolution of the fallback rate of progenitor materials with different metallicities and masses onto the accretion disk. As can be seen, the progenitor of a GRB can provide enough material to satisfy the accretion requirements of the BH obtained through fitting.

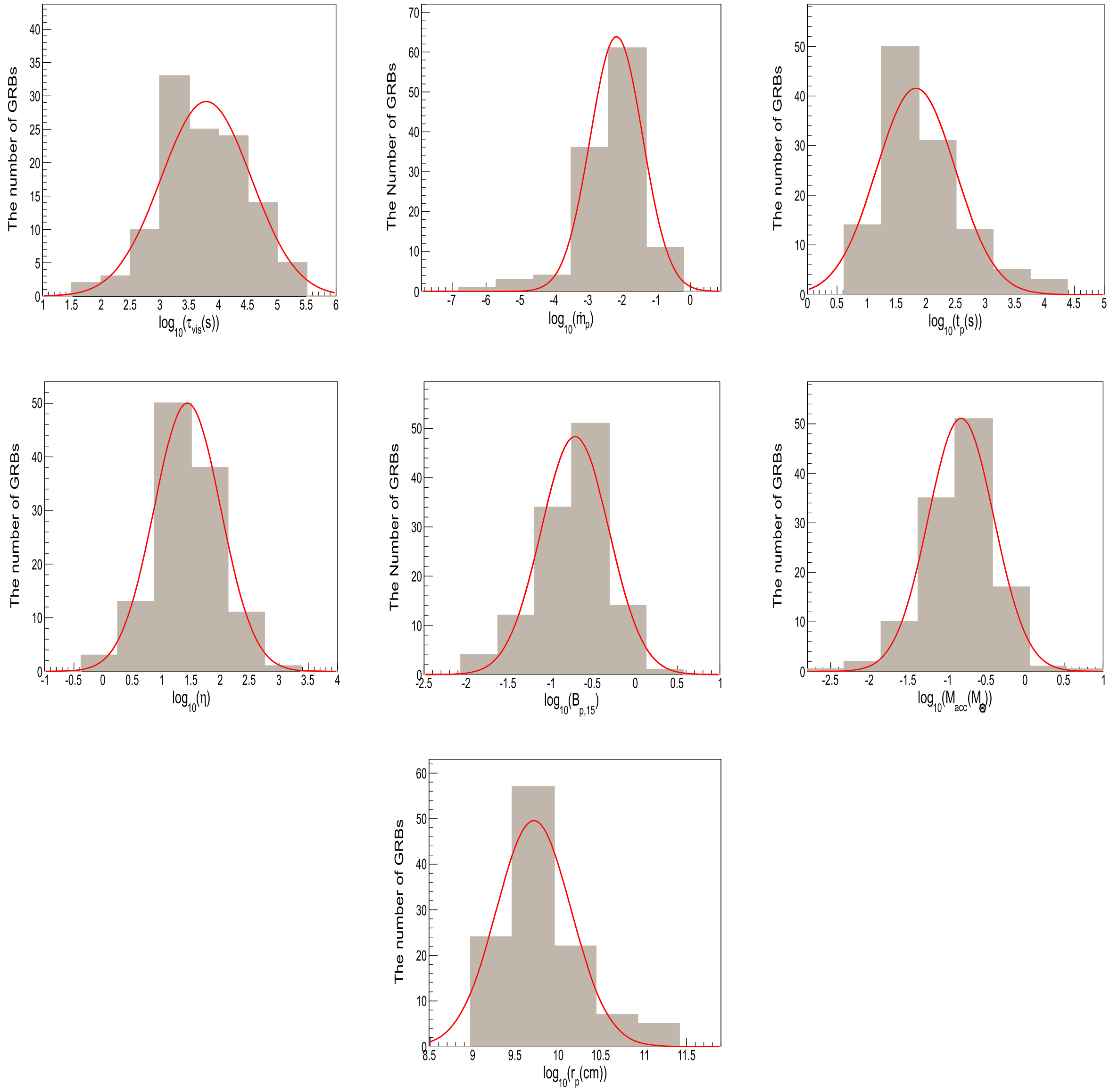

Figure 4. The distribution of $\tau_{\rm vis}$, $\dot{m}_p$, t_p, η, $B_{p,15}$, $M_{\rm acc}$, and r_p of all GRBs in our sample. The red solid line represents log-normal fitting results.

6. Discussion and Conclusion

The X-ray afterglow of most GRBs consists of a shallow decay segment, but its origin remains a mystery. E.-W. Liang et al. (2007) and L. Zhao et al. (2019) found through their research that there is no significant spectral evolution between the shallow decay segment and the follow-up segment for most GRBs, and the follow-up segments of most GRBs are consistent with the external shock model. Their research results suggest that the shallow decay segment may be produced by the continuous energy injection of an external shock by the long-term active GRB central engine and through the external dissipation mechanism. In this paper, we assume that the late activity of the central engine is powered by the fallback accretion of materials from the progenitor's envelope onto the hyperaccreting BH system.

Based on the observation data of Swift-XRT before 2023 June, we selected 103 GRBs with the shallow decay segment. We applied the fallback accretion energy external dissipation model to our sample and found that the model can successfully interpret the shallow decay segment within a reasonable parameter space. Based on the fitting results of the model, several conclusions can be drawn. The fallback rate of the progenitor envelope materials onto the accretion disk can reach a peak of 10^{-7}–0.1 $M_\odot$ s^{-1} at a time of 10–10^5 s, which is compatible with the typical density profile and typical spin profile of the progenitor of a GRB. During the fallback process of progenitor envelope materials, most GRB progenitors have the highest fallback rate at a radius ~ 10^{10} cm, which is consistent with the typical radius of a Wolf–Rayet star. The production of shallow decay segments for most GRBs in our sample requires the injection of BZ energy that 10–100 times the kinetic energy of the initial GRB blast wave into the blast wave. However, the shallow decay segment of a few GRBs requires the injected energy to be comparable to the kinetic energy of the blast wave, suggesting that even with less energy injected into the GRB blast wave, a shallow decay segment can still be produced. In addition, the peak time of the fallback rate of the progenitor envelope materials is close to the time when BZ energy is injected into the shock wave, which means that the fallback accretion is more active during the initial phase. In

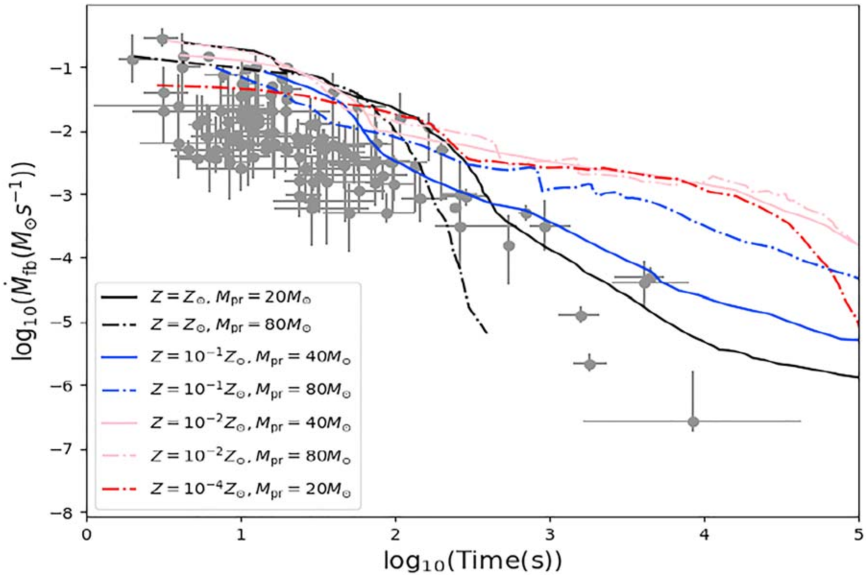

Figure 5. The evolution of the fallback rate of progenitor materials with different mass and metallicity onto the accretion disk, where $Z_\odot$ is the metallicity of the Sun, and the gray dots represent the peak of the fallback rate $\dot{m}_p$ with respect to the peak accretion time t_p.

summary, our research results further support the origin of the shallow decay segment as being due to an external shock.

In this paper, we adopt a simple BPL function to describe the evolution of the fallback rate. In fact, the density profile and spin profile of the progenitor star significantly influence the evolution of the fallback rate of envelope materials. Therefore, it is necessary to incorporate the density profile and spin profile into the fallback accretion model in the future. Studying the shallow decay segment based on the reconstructed fallback accretion model will provide a new perspective and deeper understanding of the properties of GRB progenitor stars and central engines.

As of now, the shallow decay segment of X-ray afterglow can be interpreted as being due to both the mechanism of fallback accretion onto the BH and the spin-down mechanism of rapidly rotating magnetars. It is difficult to discern which physical mechanism is more reasonable based on the properties of the shallow decay segment of X-ray afterglow alone. In the future, multiband studies of the shallow decay segment by using data from gravitational wave observations will help unravel the mystery of its formation.

Acknowledgments

We thank H. Gao for helpful discussion and the referee for helpful comments, which led to improvements of the paper. This work is supported by the National Natural Science Foundation of China under grant No. 12403047, Hebei Natural Science Foundation under grant No. A2024403004, and National Pre-research Funds of Hebei GEO University in 2024 (grant No. KY2024QN05).

Software: XSPEC (K. A. Arnaud 1996), HEAsoft (v6.12; Nasa High Energy Astrophysics Science Archive Research Center (Heasarc) 2014), root (v5.34; R. Brun & F. Rademakers 1997), emcee (v3.0rc2; D. Foreman-Mackey et al. 2013), corner (v2.0.1; D. Foreman-Mackey 2016).

ORCID iDs

Litao Zhao https://orcid.org/0000-0001-6437-0869

References

Antonelli, L.A., Maund, J.R., Palazzi, E., et al. 2010, GCN, 10620
Arnaud, K.A. 1996, in ASP Conf. Ser. 101, Astronomical Data Analysis Software and Systems V, ed. G. H. Jacoby & J. Barnes (San Francisco, CA: ASP), 17
Barbier, L., Barthelmy, S., Cummings, J., et al. 2006a, GCN, 4518
Barbier, L., Barthelmy, S., Cummings, J., et al. 2006b, GCN, 5403
Barbier, L., Barthelmy, S.D., Cummings, J., et al. 2007, GCN, 5991
Barthelmy, S. D., Barbier, L., Cummings, J.R., et al. 2007a, GCN, 6173
Barthelmy, S. D., Barbier, L., Cummings, J.R., et al. 2007b, GCN, 6390
Barthelmy, S. D., Baumgartner, W., Cummings, J.R., et al. 2008a, GCN, 7606
Barthelmy, S. D., Baumgartner, W., Cummings, J.R., et al. 2008b, GCN, 8188
Barthelmy, S.D., Baumgartner, W., Cummings, J.R., et al. 2009, GCN, 10103
Barthelmy, S.D., Baumgartner, W., Cummings, J.R., et al. 2011, GCN, 11714
Barthelmy, S. D., Sakamoto, T., Markwardt, C. B., et al. 2012c, GCN, 13120
Barthelmy, S. D., Cummings, J. R., Krimm, H. A., et al. 2017a, GCN, 21796
Barthelmy, S. D., Cummings, J. R., Gehrels, N., et al. 2017b, GCN, 20596
Barthelmy, S. D., Cannizzo, J. K., Cummings, J. R., et al. 2018a, GCN, 22348
Barthelmy, S. D., Cummings, J. R., Gropp, J. D., et al. 2018b, GCN, 22599
Barthelmy, S. D., Cummings, J. R., Krimm, H. A., et al. 2019, GCN, 23685
Barthelmy, S. D., Cummings, J. R., Krimm, H. A., et al. 2020, GCN, 29116
Barthelmy, S. D., Cummings, J. R., Krimm, H. A., et al. 2021, GCN, 30186
Baumgartner, W. H., Barthelmy, S. D., Cummings, J. R., et al. 2011b, GCN, 12424
Baumgartner, W. H., Barthelmy, S. D., Cummings, J. R., et al. 2013, GCN, 15459
Belokurov, V., Walker, M. G., Evans, N. W., et al. 2009, MNRAS, 397, 1748
Berger, E., & Soderberg, A. M. 2005, GCN, 4384
Berger, E., Fox, D. B., & Cucchiara, A. 2007, GCN, 6470
Berger, E., & Rauch, M. 2008, GCN, 7389
Blandford, R. D., & Znajek, R. L. 1977, MNRAS, 179, 433
Bloom, J. S., Perley, D. A., & Chen, H. W. 2006, GCN, 5826
Bolmer, J., Knust, F., & Greiner, J. 2015, GCN, 18603
Brun, R., & Rademakers, F. 1997, NIMPA, 389, 81
Burrows, D. N., Romano, P., Falcone, A., et al. 2005, Sci, 309, 1833
Butler, N. R. 2007, ApJ, 656, 1001
Cannizzo, J. K., & Gehrels, N. 2009, ApJ, 700, 1047
Cannizzo, J. K., & Gehrels, N. 2010, AAS HEAD Meeting, 11, 14.04
Cano, Z., Malesani, D., de Ugarte Postigo, A., et al. 2016, GCN, 20245
Cao, S., Dainotti, M., & Ratra, B. 2022, MNRAS, 516, 1386
Castro-Tirado, A. J., Amado, P., Negueruela, I., et al. 2006, GCN, 5218
Castro-Tirado, A. J., Cunniffe, R., Sanchez-Ramirez, R., et al. 2014, GCN, 16505
Cenko, S. B., Kulkarni, S. R., Gal-Yam, A., & Berger, E. 2005, GCN, 3542
Chen, W.-X., & Beloborodov, A. M. 2007, ApJ, 657, 383
Chen, H.-W., Helsby, J., Shectman, S., Thompson, I., & Crane, J. 2009, GCN, 10038

Chen, W., Xie, W., Lei, W.-H., et al. 2017, ApJ, 849, 119
Chevalier, R. A. 1989, ApJ, 346, 847
Chornock, R., Perley, D. A., Cenko, S. B., et al. 2009, GCN, 8994
Chornock, R., Cenko, S. B., Griffith, C. V., et al. 2009a, GCN, 9151
Chornock, R., Perley, D. A., Cenko, S. B., & Bloom, J. S. 2009b, GCN, 9243
Chornock, R., Perley, D. A., & Cobb, B. E. 2009c, GCN, 10100
Chornock, R., Cucchiara, A., Fox, D., & Berger, E. 2010a, GCN, 10466
Chornock, R., Berger, E., Fox, D., et al. 2010b, GCN, 11164
Chornock, R., Berger, E., & Fox, D. B. 2011, GCN, 11538
Chornock, R., Fox, D. B., Cucchiara, A., Perley, D. A., & Levan, A. 2014, GCN, 16301
Connaughton, V. 2009, GCN, 9230
Cucchiara, A., Price, P. A., Fox, D. B., Cenko, S. B., & Schmidt, B. P. 2006, GCN, 5052
Cucchiara, A., & Fox, D. B. 2008, GCN, 7654
Cucchiara, A., & Levan, A. J. 2011, GCN, 12761
Cummings, J. R., Barthelmy, S. D., Baumgartner, W. H., et al. 2008a, GCN, 8708
Cummings, J. R., Barthelmy, S. D., Baumgartner, W. H., et al. 2008b, GCN, 8447
Cummings, J. R., Barthelmy, S. D., Baumgartner, W. H., et al. 2009, GCN, 8886
Cummings, J. R., Barthelmy, S. D., Baumgartner, W. H., et al. 2010, GCN, 10462
Cummings, J. R., Barthelmy, S. D., Baumgartner, W. H., et al. 2011, GCN, 12749
Cummings, J. R., Barthelmy, S. D., Baumgartner, W. H., et al. 2015, GCN, 17581
Dai, Z. G., & Liu, R.-Y. 2012, ApJ, 759, 58
Dainotti, M. G., Cardone, V. F., & Capozziello, S. 2008, MNRAS, 391, L79
Dainotti, M. G., Willingale, R., Capozziello, S., Fabrizio Cardone, V., & Ostrowski, M. 2010, ApJL, 722, L215
Dainotti, M. G., Fabrizio Cardone, V., Capozziello, S., Ostrowski, M., & Willingale, R. 2011, ApJ, 730, 135
Dainotti, M. G., Cardone, V. F., Piedipalumbo, E., et al. 2013, MNRAS, 436, 82
Dainotti, M., Petrosian, V., Willingale, R., et al. 2015, MNRAS, 451, 3898
Dainotti, M. G., Postnikov, S., Hernandez, X., & Ostrowski, M. 2016, ApJL, 825, L20
Dainotti, M. G., Hernandez, X., Postnikov, S., et al. 2017, ApJ, 848, 88
Dainotti, M. G., Lenart, A., Sarracino, G., et al. 2020a, ApJ, 904, 97
Dainotti, M. G., Livermore, S., Kann, D. A., et al. 2020b, ApJL, 905, L26
Dall'Osso, S., Stratta, G., Guetta, D., et al. 2011, A&A, 526, A121
Del Vecchio, R., Dainotti, M. G., & Ostrowski, M. 2016, ApJ, 828, 36
D'Elia, V., Covino, S., & D'Avanzo, P. 2008, GCN, 8438
D'Elia, V., Goldoni, P., Malesani, D., et al. 2012, GCN, 13227
D'Elia, V., D'Avanzo, P., Covino, S., et al. 2014, GCN, 15802
De Pasquale, M., Oates, S. R., Racusin, J. L., et al. 2016, MNRAS, 455, 1027
de Ugarte Postigo, A., Fynbo, J. P. U., Thoene, C., et al. 2015, GCN, 17583
de Ugarte Postigo, A., Fynbo, J. P. U., Jakobsson, P., et al. 2011, GCN, 12258
de Ugarte Postigo, A., Tanvir, N. R., Cano, Z., et al. 2016a, GCN, 19245
de Ugarte Postigo, A., Malesani, D., Perley, D. A., et al. 2016b, GCN, 20150
de Ugarte Postigo, A., Izzo, L., Thoene, C., et al. 2017a, GCN, 20584
de Ugarte Postigo, A., Izzo, L., Thoene, C. C., et al. 2017b, GCN, 21799
de Ugarte Postigo, A., Izzo, L., Kann, D. A., et al. 2017c, GCN, 22272
de Ugarte Postigo, A., Kann, D. A., Izzo, L., et al. 2017d, GCN, 21298
de Ugarte Postigo, A., Cano, Z., Izzo, L., et al. 2018, GCN, 22346
de Ugarte Postigo, A., Tanvir, N. R., Xu, D., et al. 2019, GCN, 23680
de Ugarte Postigo, A., Kann, D. A., Thoene, C. C., et al. 2021, GCN, 29450
Di Matteo, T., Perna, R., & Narayan, R. 2002, ApJ, 579, 706
Evans, P. A., Beardmore, A. P., Page, K. L., et al. 2009, MNRAS, 397, 1177
Fenimore, E., Barbier, L., Barthelmy, S. D., et al. 2006, GCN, 5831
Fenimore, E. E., Barthelmy, S. D., Baumgartner, W. H., et al. 2009, GCN, 9157
Filgas, R., Tautenburg, T., Kupcu-Yoldas, A., et al. 2008, GCN, 7747
Foreman-Mackey, D., Hogg, D. W., Lang, D., & Goodman, J. 2013, PASP, 125, 306
Foreman-Mackey, D. 2016, JOSS, 1, 24
Fugazza, D., Malesani, D., Romano, P., et al. 2006, GCN, 5276
Fugazza, D., Thoene, C. C., D'Elia, V., et al. 2009, GCN, 8892
Fynbo, J. P. U., Hjorth, J., Jensen, B. L., et al. 2005a, GCN, 3136
Fynbo, J. P. U., Jensen, B. L., Hjorth, J., et al. 2005b, GCN, 3176
Fynbo, J. P. U., Sollerman, J., Jensen, B. L., et al. 2005c, GCN, 3749
Fynbo, J. P. U., Jensen, B. L., Sollerman, J., et al. 2005d, GCN, 3874
Fynbo, J. P. U., Malesani, D., & Milvang-Jensen, B. 2008, GCN, 7949
Fynbo, J. P. U., Jakobsson, P., Prochaska, J. X., et al. 2009, ApJS, 185, 526
Gao, H., Lei, W.-H., You, Z.-Q., et al. 2016b, ApJ, 826, 141
Goldoni, P., Flores, H., Malesani, D., et al. 2010, GCN, 10684
Goldoni, P., de Ugarte Postigo, A., & Fynbo, J. P. U. 2013, GCN, 15571
Golenetskii, S., Aptekar, R., Mazets, E., et al. 2005, GCN, 4394
Golenetskii, S., Aptekar, R., Mazets, E., et al. 2006a, GCN, 5264
Golenetskii, S., Aptekar, R., Mazets, E., et al. 2006b, GCN, 5460
Golenetskii, S., Aptekar, R., Mazets, E., et al. 2006c, GCN, 5837
Golenetskii, S., Aptekar, R., Mazets, E., et al. 2007, GCN, 6403
Gompertz, B. P., van der Horst, A. J., O'Brien, P. T., Wynn, G. A., & Wiersema, K. 2015, MNRAS, 448, 629
Gu, W.-M., Liu, T., & Lu, J.-F. 2006, ApJL, 643, L87
Halpern, J. P., & Mirabal, N. 2006, GCN, 5982
Hjorth, J., Malesani, D., Jakobsson, P., et al. 2012, ApJ, 756, 187
Huang, Y. F., Gou, L. J., Dai, Z. G., & Lu, T. 2000, ApJ, 543, 90
Hullinger, D., Angelini, L., Barbier, L., et al. 2005, GCN, 3856
Hullinger, D., Angelini, L., Barbier, L., et al. 2006, GCN, 4851
Izzo, L., Arabsalmani, M., Malesani, D. B., et al. 2018, GCN, 22823
Jakobsson, P., Tanvir, N., Jensen, B. L., et al. 2006a, GCN, 5298
Jakobsson, P., Vreeswijk, P., Fynbo, J. P. U., et al. 2006b, GCN, 5320
Jakobsson, P., Fynbo, J. P. U., Andersen, M. I., et al. 2007, GCN, 6398
Janiuk, A., Perna, R., Di Matteo, T., et al. 2004, MNRAS, 355, 950
Jaunsen, A. O., Thoene, C. C., Fynbo, J. P. U., Hjorth, J., & Vreeswijk, P. 2007b, GCN, 6202
Kawanaka, N., Piran, T., & Krolik, J. H. 2013, ApJ, 766, 31
Krimm, H., Sakamoto, T., Barthelmy, S., et al. 2005a, GCN, 3119
Krimm, H., Barbier, L., Barthelmy, S., et al. 2005b, GCN, 3871
Krimm, H., Barbier, L., Barthelmy, S. D., et al. 2006c, GCN, 5334
Krimm, H., Barbier, L., Barthelmy, S. D., et al. 2007, GCN, 6058
Krimm, H., Barthelmy, S. D., Baumgartner, W., et al. 2008, GCN, 7736
Krimm, H. A., Barlow, B. N., Barthelmy, S. D., et al. 2012, GCN, 13634
Krimm, H. A., Barthelmy, S. D., Baumgartner, W. H., et al. 2014a, GCN, 16200
Krimm, H. A., Barthelmy, S. D., Baumgartner, W. H., et al. 2014b, GCN, 16509
Krimm, H. A., Barthelmy, S. D., Baumgartner, W. H., et al. 2014c, GCN, 17083
Krimm, H. A., Barthelmy, S. D., Cummings, J. R., et al. 2015, GCN, 18593
Krimm, H. A., Barthelmy, S. D., Cummings, J. R., et al. 2016, GCN, 19765
Krimm, H. A., Barthelmy, S. D., Cummings, J. R., et al. 2017, GCN, 21296
Kruehler, T., Malesani, D., de Ugarte Postigo, A., Melandri, A., & Fynbo, J. P. U. 2014, GCN, 16194
Krühler, T., Malesani, D., Milvang-Jensen, B., et al. 2012, ApJ, 758, 46
Kumar, P., Narayan, R., & Johnson, J. L. 2008, MNRAS, 388, 1729
Kumar, P., & Johnson, J. L. 2010, MNRAS, 404, 2170
Lee, H. K., Wijers, R. A. M. J., & Brown, G. E. 2000, PhR, 325, 83
Lei, W.-H., & Zhang, B. 2011, ApJL, 740, L27
Lei, W.-H., Wang, D.-X., & Ma, R.-Y. 2005, ApJ, 619, 420
Lei, W. H., Wang, D. X., Zhang, L., et al. 2009, ApJ, 700, 1970
Lei, W.-H., Zhang, B., & Liang, E.-W. 2013, ApJ, 765, 125
Lei, W.-H., Zhang, B., Wu, X.-F., & Liang, E.-W. 2017, ApJ, 849, 47
Li, L.-X. 2000, PhRvD, 084016, 61
Liang, E.-W., Zhang, B.-B., & Zhang, B. 2007, ApJ, 670, 565
Lien, A. Y., Barthelmy, S. D., Cummings, J. R., et al. 2015, GCN, 18268
Lien, A. Y., Barthelmy, S. D., Cummings, J. R., et al. 2018, GCN, 23321
Lien, A. Y., Barthelmy, S. D., Krimm, H. A., et al. 2021, GCN, 29467
Lien, A. Y., Barthelmy, S. D., Krimm, H. A., et al. 2023, GCN, 33523
Liu, T., Gu, W.-M., Xue, L., et al. 2007, ApJ, 661, 1025
Liu, T., Hou, S.-J., Xue, L., et al. 2015, ApJS, 218, 12
Liu, T., Gu, W.-M., & Zhang, B. 2017, NewAR, 79, 1
Liu, T., Song, C.-Y., Zhang, B., Gu, W.-M., & Herger, A. 2018, ApJ, 852, 20
Lloyd-Ronning, N. M., Lei, W.-H., & Xie, W. 2018, MNRAS, 478, 3525
Lü, H.-J., & Zhang, B. 2014, ApJ, 785, 74
Lyons, N., O'Brien, P. T., Zhang, B., et al. 2010, MNRAS, 402, 705
MacFadyen, A. I., & Woosley, S. E. 1999, ApJ, 524, 262
MacFadyen, A. I., Woosley, S. E., & Heger, A. 2001, ApJ, 550, 410
Malesani, D., Fynbo, J. P. U., D'Elia, V., et al. 2009, GCN, 9457
Malesani, D., Kruehler, T., Perley, D., et al. 2013, GCN, 14225
Markwardt, C., Barbier, L., Barthelmy, S., et al. 2005, GCN, 3888
Markwardt, C., Barbier, L., Barthelmy, S. D., et al. 2007, GCN, 6748
Markwardt, C. B., Barthelmy, S. D., Baumgartner, W. H., et al. 2009a, GCN, 9434
Markwardt, C. B., Barthelmy, S. D., Baumgartner, W. H., et al. 2009b, GCN, 1040
Markwardt, C. B., Barthelmy, S. D., Baumgartner, W. H., et al. 2010, GCN, 10685

Markwardt, C. B., Barthelmy, S. D., Baumgartner, W. H., et al. 2012, GCN, 13333
Markwardt, C. B., Amaral-Rogers, A., Barthelmy, S. D., et al. 2015, GCN, 17628
Markwardt, C. B., Barthelmy, S. D., Cummings, J. R., et al. 2016, GCN, 19240
Markwardt, C. B., Barthelmy, S. D., Cummings, J. R., et al. 2017, GCN, 20456
McKinney, J. C. 2005, ApJL, 630, L5
Melandri, A., Grazian, A., Guidorzi, C., et al. 2006, GCN, 4539
Milne, P. A., & Cenko, S. B. 2011, GCN, 11708
Moderski, R., Sikora, M., & Lasota, J. P. 1997, Relativistic Jets in AGNs (Berlin: Springer), 110
Mooley, K. P., Staley, T. D., Fender, R. P., et al. 2016, GCN, 20200
Narayan, R., Piran, T., & Kumar, P. 2001, ApJ, 557, 949
Nasa High Energy Astrophysics Science Archive Research Center (Heasarc), 2014 HEAsoft: Unified Release of FTOOLS and XANADU, Astrophysics Source Code Library, ascl:1408.004
Nousek, J. A., Kouveliotou, C., Grupe, D., et al. 2006, ApJ, 642, 389
Novikov, I. D., & Thorne, K. S. 1973, Black Holes (Les Astres Occlus) (London: Gordon and Breach), 343
O'Brien, P. T., Willingale, R., Osborne, J., et al. 2006, ApJ, 647, 1213
O'Brien, P. T., & Rowlinson, A. 2012, in IAU Symp. 279, Death of Massive Stars: Supernovae and Gamma-Ray Bursts (Cambridge: Cambridge Univ. Press), 297
Paczyński, B. 1998, ApJL, 494, L45
Palmer, D., Barbier, L., Barthelmy, S., et al. 2005, GCN, 3737
Palmer, D., Barbier, L., Barthelmy, S. D., et al. 2006, GCN, 5551
Palmer, D., Barbier, L., Barthelmy, S. D., et al. 2007, GCN, 6440
Palmer, D. M., Barthelmy, S. D., Baumgartner, W. H., et al. 2009, GCN, 9443
Palmer, D. M., Barthelmy, S. D., Baumgartner, W. H., et al. 2012, GCN, 14011
Palmer, D. M., Barthelmy, S. D., Baumgartner, W. H., et al. 2014, GCN, 16240
Palmer, D. M., Barthelmy, S. D., Cummings, J. R., et al. 2015, GCN, 18496
Palmer, D. M., Barthelmy, S. D., Beardmore, A. P., et al. 2016, GCN, 20151
Palmer, D. M., Barthelmy, S. D., Cummings, J. R., et al. 2017, GCN, 22280
Palmer, D. M., Barthelmy, S. D., Cummings, J. R., et al. 2018, GCN, 22566
Palmer, D. M., Barthelmy, S. D., Cummings, J. R., et al. 2019, GCN, 23625
Palmer, D. M., Barthelmy, S. D., Krimm, H. A., et al. 2021, GCN, 29251
Parsons, A., Barthelmy, S., Burrows, D., et al. 2005, GCN, 4363
Parsons, A., Barbier, L., Barthelmy, S., et al. 2006a, GCN, 5053
Parsons, A., Barbier, L., Barthelmy, S., et al. 2006b, GCN, 5214
Parsons, A., Barbier, L., Barthelmy, S. D., et al. 2006c, GCN, 5370
Parsons, A., Barbier, L., Barthelmy, S. D., et al. 2007, GCN, 6468
Perley, D. A., & Cenko, S. B. 2015, GCN, 17616
Perley, D. A., Levan, A. J., Tanvir, N. R., et al. 2013, ApJ, 778, 128
Perley, D. A., Ott, C. P., Modjaz, M., & Fierroz, D. 2014, GCN, 17081
Perley, D. A., Hillenbrand, L., & Prochaska, J. X. 2015, GCN, 18487
Pieterse, D., Fynbo, J. P. U., Izzo, L., et al. 2023, GCN, 33521
Piranomonte, S., D'Elia, V., Fiore, F., et al. 2006, GCN, 4520
Popham, R., Woosley, S. E., & Fryer, C. 1999, ApJ, 518, 356
Pugliese, V., Xu, D., Tanvir, N. R., et al. 2015, GCN, 17672
Rea, N., Gullón, M., Pons, J. A., et al. 2015, ApJ, 813, 92
Rowlinson, A., O'Brien, P. T., Tanvir, N. R., et al. 2010, MNRAS, 409, 531
Rowlinson, A., O'Brien, P. T., Metzger, B. D., Tanvir, N. R., & Levan, A. J. 2013, MNRAS, 430, 1061
Rowlinson, A., Gompertz, B. P., Dainotti, M., et al. 2014, MNRAS, 443, 1779
Rybicki, G. B., & Lightman, A. P. 1979, A Wiley-Interscience Publication (New York: Wiley)
Sakamoto, T., Barthelmy, S., Barbier, L., et al. 2005a, GCN, 3173
Sakamoto, T., Barbier, L., Barthelmy, S., et al. 2005b, GCN, 3273
Sakamoto, T., Barbier, L., Barthelmy, S., et al. 2006a, GCN, 4445
Sakamoto, T., Barbier, L., Barthelmy, S. D., et al. 2006b, GCN, 5349
Sakamoto, T., Barbier, L., Barthelmy, S. D., et al. 2006c, GCN, 5534
Sakamoto, T., Hill, J. E., Yamazaki, R., et al. 2007, ApJ, 669, 1115
Sakamoto, T., Barthelmy, S. D., Baumgartner, W. H., et al. 2009, GCN, 8986
Sakamoto, T., Barthelmy, S. D., Baumgartner, W. H., et al. 2010, GCN, 11169
Sakamoto, T., Barthelmy, S. D., Baumgartner, W. H., et al. 2011, GCN, 12262
Sakamoto, T., Barthelmy, S. D., Baumgartner, W. H., et al. 2012, GCN, 12873
Sakamoto, T., Barthelmy, S. D., Baumgartner, W. H., et al. 2014, GCN, 15805
Sakamoto, T., Barthelmy, S. D., Baumgartner, W. H., et al. 2015, GCN, 17675
Sakamoto, T., Barthelmy, S. D., Cummings, J. R., et al. 2016, GCN, 19106
Sanchez-Ramirez, R., Gorosabel, J., de Ugarte Postigo, A., & Gonzalez Perez, J. M. 2012, GCN, 13723
Sanchez-Ramirez, R., Oates, S. R., Tello, J. C., et al. 2016, GCN, 18925
Sari, R., Piran, T., & Narayan, R. 1998, ApJL, 497, L17
Sarin, N., Lasky, P. D., & Ashton, G. 2020, PhRvD, 101, 063021
Sato, G., Barbier, L., Barthelmy, S., et al. 2006a, GCN, 5231
Sato, G., Sakamoto, T., Markwardt, C., et al. 2006b, GCN, 5538
Schady, P., & Marshall, F. E. 2008, GCN, 7953
Schady, P., Xu, D., Heintz, K. E., et al. 2019, GCN, 23632
Selsing, J., Malesani, D., Kann, D. A., et al. 2018, GCN, 22591
Srinivasaragavan, G. P., Dainotti, M. G., Fraija, N., et al. 2020, ApJ, 903, 18
Stamatikos, M., Barbier, L., Barthelmy, S., et al. 2006, GCN, 5289
Stamatikos, M., Barthelmy, S. D., Baumgartner, W., et al. 2008, GCN, 7656
Stamatikos, M., Barthelmy, S. D., Baumgartner, W. H., et al. 2012, GCN, 13720
Still, A., Kniazev, M., Romero-Colmenero, E., et al. 2006, GCN, 5226
Stratta, G., Dainotti, M. G., Dall'Osso, S., et al. 2018, ApJ, 869, 155
Tagliaferri, G., Goad, M., Chincarini, G., et al. 2005, Natur, 436, 985
Tanvir, N. R., Levan, A. J., & Matulonis, T. 2012a, GCN, 14009
Tanvir, N. R., Wiersema, K., Levan, A. J., et al. 2012b, GCN, 13348
Tello, J. C., Sanchez-Ramirez, R., Gorosabel, J., et al. 2012, GCN, 13118
Thoene, C. C., Perley, D. A., Cooke, J., et al. 2007, GCN, 6741
Thoene, C. C., de Ugarte Postigo, A., Gorosabel, J., et al. 2012, GCN, 13628
Troja, E., Cusumano, G., O'Brien, P. T., et al. 2007, ApJ, 665, 599
Tueller, J., Barthelmy, S., Barbier, L., et al. 2005, GCN, 3615
Tueller, J., Barthelmy, S. D., Cummings, J., et al. 2008, GCN, 7402
Tueller, J., Barthelmy, S. D., Baumgartner, W. H., et al. 2009a, GCN, 8808
Tueller, J., Barthelmy, S. D., Baumgartner, W. H., et al. 2009b, GCN, 9089
Ukwatta, T. N., Barthelmy, S. D., Baumgartner, W. H., et al. 2009, GCN, 9104
Ukwatta, T. N., Barthelmy, S. D., Baumgartner, W. H., et al. 2010, GCN, 10615
Ukwatta, T. N., Barthelmy, S. D., Baumgartner, W. H., et al. 2011, GCN, 11533
Ukwatta, T. N., Barthelmy, S. D., Baumgartner, W. H., et al. 2012, GCN, 13220
Ukwatta, T. N., Barthelmy, S. D., Baumgartner, W. H., et al. 2014, GCN, 16306
Ukwatta, T. N., Barthelmy, S. D., Cummings, J. R., et al. 2018, GCN, 22821
Veres, P. & Fermi-GBM Team 2020, GCN, 29110
Vielfaure, J.-B., Japelj, J., Malesani, D. B., et al. 2018, GCN, 23315
Vreeswijk, P., Jakobsson, P., Ledoux, C., Thoene, C., & Fynbo, J. 2006, GCN, 5535
Vreeswijk, P. M., Thoene, C. C., Malesani, D., et al. 2008a, GCN, 7601
Vreeswijk, P. M., Fynbo, J. P. U., Malesani, D., Hjorth, J., & de Ugarte Postigo, A. 2008b, GCN, 8191
Wang, D. X., Xiao, K., & Lei, W. H. 2002, MNRAS, 335, 655
Wiersema, K., Flores, H., D'Elia, V., et al. 2011, GCN, 12431
Willingale, R., O'Brien, P. T., Osborne, J. P., et al. 2007, ApJ, 662, 1093
Willingale, R., Genet, F., Granot, J., et al. 2010, MNRAS, 403, 1296
Woosley, S. E., & Bloom, J. S. 2006, ARA&A, 44, 507
Woosley, S. E. 1993, ApJ, 405, 273
Wu, X.-F., Hou, S.-J., & Lei, W.-H. 2013, ApJL, 767, L36
Xie, W., Lei, W.-H., & Wang, D.-X. 2016, ApJ, 833, 129
Xie, W., Lei, W.-H., & Wang, D.-X. 2017, ApJ, 838, 143
Xu, D., Malesani, D., Tanvir, N., et al. 2013, GCN, 15450
Xu, D., Fynbo, J. P. U., Malesani, D., et al. 2016a, GCN, 19109
Xu, D., Heintz, K. E., Malesani, D., Wiersema, K., & Fynbo, J. P. U. 2016b, GCN, 19773
Xu, D., Heintz, K. E., Malesani, D., & Fynbo, J. P. U. 2017, GCN, 20458
Yu, Y. B., Wu, X. F., Huang, Y. F., et al. 2015, MNRAS, 446, 3642
Zhang, B., Fan, Y. Z., Dyks, J., et al. 2006, ApJ, 642, 354
Zhang, B., Liang, E., Page, K. L., et al. 2007, ApJ, 655, 989
Zhang, B., Lei, W.-H., Li, Y., & Lasky, P. D. 2015, ApJ, 805, 89
Zhang, B. 2018, The Physics of Gamma-Ray Bursts (Cambridge: Cambridge Univ. Press),
Zhang, L.-L., Xin, L.-P., Wang, J., et al. 2022, ApJ, 941, 63
Zhang, Q., Huang, Y. F., & Zong, H. S. 2016, ApJ, 823, 156
Zhang, W., Woosley, S. E., & Heger, A. 2008, ApJ, 679, 639
Zhao, L., Zhang, B., Gao, H., et al. 2019, ApJ, 883, 9
Zhao, L., Liu, L., Gao, H., et al. 2020, ApJ, 896, 42
Zheng, W., Filippenko, A. V., Yuk, H., Zhu, Y., & Perley, D. A. 2015, GCN, 18273
Zhu, Z. P., Xu, D., Fu, S. Y., et al. 2021, GCN, 30164